2007

Petrology and Geochemistry of the AND-1B Core, ANDRILL McMurdo Ice Shelf Project, Antarctica

M. Pompilio
Istituto Nazionale di Geofisica e Vulcanologia, pompilio@pi.ingv.it

N. Dunbar
New Mexico Institute of Technology

A. C. Gebhardt
Alfred Wegener Institute for Polar and Marine Research

D. Helling
Alfred Wegener Institute for Polar and Marine Research

G. Kuhn
Wegener Institute for Polar and Marine Research, gkuhn@awi-bremerhaven.de

See next page for additional authors

Terra Antartica
2007, **14**(3), 255-288

TERRA ANTARTICA
AN ANTARCTIC EARTH SCIENCE JOURNAL

Petrology and Geochemistry of the AND-1B Core, ANDRILL McMurdo Ice Shelf Project, Antarctica

M. Pompilio[1], N. Dunbar[2], A.C. Gebhardt[3], D. Helling[3], G. Kuhn[3], P. Kyle[2], R. McKay[4], F.Talarico[5], S. Tulaczyk[6], S. Vogel[7], T. Wilch[8] & the ANDRILL-MIS Science Team[9]

[1]Istituto Nazionale di Geofisica e Vulcanologia, I-56126 Pisa - Italy
[2]Earth and Environmental Science Department, New Mexico Institute of Technology, Socorro, NM 87801 - USA
[3]Alfred Wegener Institute for Polar and Marine Research, D-27515, Bremerhaven - Germany
[4]Antarctic Research Centre, Victoria University of Wellington, PO Box 600, Wellington - New Zealand
[5]Università di Siena, Dipartimento di Scienze delle Terra, I-53100 Siena - Italy
[6]Department of Earth Sciences, University of California at Santa Cruz, Santa Cruz, CA 95064 - USA
[7]Department of Geology and Environmental Geosciences, Northern Illinois University, DeKalb, IL 60115 - USA
[8]Department of Geology, Albion College, Albion, MI 49224 - USA
[9]http://www.andrill.org/support/references/appendixc.html

**Corresponding author* (pompilio@pi.ingv.it)

Abstract - This section reports preliminary data and results on petrology and geochemistry of AND-1B core.

INTRODUCTION

Petrologic descriptions will follow a division related to both grain size and lithology like that adopted in Cape Roberts investigation (Cape Roberts Science Team 2000, and references therein). First, we describe the petrology of the sand fraction of the core. Second, we report the distribution of clasts with diameter larger than 2 millimetre (mm) and the petrology of basement clasts. Third, we focus on the occurrence and petrology of McMurdo Volcanic Group sediments, which represent the largest component in the core.

The final section continues with the compositional characterisation of bulk sediments by continuous X-ray fluorescence measurement (XRF scan) integrated by carbonate geochemistry and concludes with the pore-water geochemistry. All of these data will contribute to infer palaeoclimatic information and to understand provenance history of detritus, changes in depositional environment, and spatial and temporal evolution of magmatism in McMurdo Ice Shelf area.

PETROLOGY OF SAND FRACTION

The sand-size fraction was petrologically analysed to identify potential changes in provenance among facies and with depth. Visual estimates were used in this initial description of the sand-fraction petrology from thin sections of diamictites, sandstones, and other facies of interest. The results given here are qualitative and are used to assist initial core characterisation. Quantitative analysis of the sand fraction will follow particle size analyses.

METHODS

A total of 52 thin sections were examined from lithostratigraphic units (LSUs) 1–6 to determine changes in provenance and sedimentary processes (Tab. 1). On-ice time did not allow for thin-section preparation from LSUs 7 and 8 at the base of the core. The majority of the samples are from stratified or massive diamictites, sandstone, or sand-bearing mudstones. Samples were impregnated with epoxy resin and cut into unstained and uncovered thin sections. Identifying microfabric structures within diamictites proved difficult, as the epoxy failed to penetrate many samples and/or the diagenetic overprint distorted the original fabric. These two factors were also a problem for gaining meaningful qualitative results from the smear slides. Visual estimates were used to determine abundances of mineral and lithic fragments, and the results are given in table 1. Visual estimates of volcanic glass abundance were recorded during smear analysis for initial core description, and are shown in figure 1.

RESULTS

There is wide variability in the mineral assemblages throughout the core, and they appear to be strongly facies dependent. Previous petrological studies from sediment gravity cores taken from beneath the McMurdo Ice Shelf at a nearby site indicated that glacially derived diamicts (deposited during retreat of Last Glacial Maximum [LGM] ice) have a strong Transantarctic Mountain (TAM) provenance signal, whereas Holocene muds and sands are dominated by McMurdo Volcanic Group sediments (Barrett et

Tab. 1 - Visual estimates of mineral and matrix percentages from thin sections.

Lithostratigraphic Unit	Depth (mbsf)	Facies	Rounded Qtz	Angular Qtz	Polycrystalline Qtz	Volcanic Rock Fragments	Volcanic Glass	Microcline	Feldspar	Sed Rock Fragments	Met Sed Fragments	Plutonic rock fragments	Pyroxene (no cleavage)	Pyroxene (cleavage)	Amphibole	Biotite	Opaques	Carbonates	Matrix
1.1	24.4	*3*	-	-	-	15	80	-	3	-	-	-	1	-	T	-	-	1	-
	24.6	*3*	-	-	-	5	80	-	10	-	-	-	5	-	-	-	-	-	-
	24.7	*3*	-	-	-	30	40	-	25	-	-	-	4	-	1	-	-	-	-
	25.9	*3*	-	5	1	5	-	7	5	1	-	-	1	-	1	-	-	-	74
	48.0	*7*	5	3	-	5	T	3	10	-	2	5	-	-	-	-	-	3	64
	35.8	*9*	10	10	-	10	10	5	15	5	10	-	T	-	T	-	-	3	22
	26.7	*10*	1	5	1	10	-	5	5	T	1	-	1	-	T	-	-	-	71
	28.9	*10*	-	5	-	2	-	7.5	-	1	1	1	1	-	T	-	T	-	81
	31.2	*10*	1	2	T	7	5	-	5	-	T	-	T	-	-	-	-	-	80
	66.6	*10*	3	6	2	2	T	T	7	2	1	3	T	-	-	-	-	1	73
	70.8	*10*	-	5	-	2	-	-	5	-	5	1	T	-	-	-	-	3	79
	74.7	*10*	-	5	-	2	-	-	5	-	5	-	T	-	-	-	-	3	80
3.1	316.2	*1*	2	10	T	10	5	-	5	1	-	-	T	T	-	-	1	1	65
	296.7	*2a*	-	-	-	-	T	-	1.5	-	-	-	-	-	-	-	0.5	1	97
	224.7	*3*	-	-	-	5	7.5	-	10	-	-	-	1	-	T	-	1.5	-	75
	358.9	*3*	-	2.5	-	5	5	-	12.5	30	-	-	1	-	-	-	1	T	43
3.3	361.6	*3*	-	2.5	-	7.5	15	-	20	1	-	-	1	-	T	-	-	-	53
	151.0	*4*	-	-	-	1	1	-	0.5	-	-	-	T	-	T	-	-	-	97.5
	151.5	*4*	-	-	-	2	2	-	1	-	-	-	T	-	T	-	T	-	95
	148.3	*9*	-	5	-	5	7.5	-	5	-	-	T	T	-	T	-	-	1	76
	150.4	*9*	-	5	-	4	1	-	7.5	-	2.5	1	1	-	1	-	-	2	75
3.4	181.9	*9*	-	10	-	T	T	-	10	2.5	10	2.5	T	-	T	-	-	T	65
	225.4	*10*	-	1	-	2	1	-	5	-	T	-	T	-	T	-	1	-	90
	238.7	*10*	T	3	-	10	5	-	5	-	-	T	-	T	-	-	1	T	76
	307.4	*10*	-	2	-	2	3	-	7.5	-	T	-	T	-	-	-	1.5	-	84
3.5	337.0	*10*	-	2.5	-	2.5	2.5	-	10	-	-	1	1	-	0.5	-	1	-	79
	375.4	*10*	1	5	1	2	2.5	-	5	1	-	T	T	-	T	T	-	1	81.5
	191.2	*1+10*	-	-	-	1	2	-	5	1	-	-	T	-	T	-	1	T	90
3.6	348.2	*2a+10*	2.5	-	-	10	10	-	7.5	10	1	-	1	-	1	-	1	1	55
4.3	545.5	*4*	-	2.5	-	T	7.5	T	5	-	-	-	-	-	-	-	T	1	84
	578.5	*6*	-	10	-	-	-	-	10	2.5	-	-	1	-	-	T	20	50	6
4.4	524.0	*4+9*	T	2	-	5	10	T	5	1	T	-	T	-	-	T	T	T	77
5.1	596.7	*6V*	-	T	-	-	30	-	5	-	-	-	T	-	-	-	2.5	50	12
5.3	677.1	*8V*	-	-	-	15	30	-	-	-	-	-	5	-	-	-	-	-	50
5.4	750.8	*9*	5	20	5	T	T	-	5	T	-	-	-	-	-	-	-	-	65
6.1	820.5	*3*	1	2.5	-	-	5	-	2.5	35	-	-	5	-	-	-	T	-	49
	778.9	*4*	-	-	-	-	T	-	1	T	-	-	-	-	-	-	-	T	99
	979.0	*4*	1	5	1	-	8	-	5	7.5	7.5	T	-	T	-	-	-	1	64
	1009.4	*4*	T	1	-	T	5	-	2.5	2.5	-	1	-	-	-	-	-	7.5	80
	1033.6	*5*	-	2.5	-	-	T	-	5	-	-	-	-	T	-	-	-	-	92.5
	791.6	*7*	5	-	-	15	25	-	5	5	5	20	-	-	-	-	-	T	20
	819.7	*7*	-	1	-	1	5	-	2	40	-	-	T	-	-	-	1	T	50
	827.2	*7*	-	5	-	5	5	-	10	-	-	-	2	-	-	-	-	T	73
	830.6	*9*	-	T	-	-	20	-	5	-	-	-	T	-	-	-	T	-	75
6.3	853.3	*9*	1	5	1	5	-	-	5	1	1	1	-	-	-	-	-	-	80
	778.7	*10*	5	20	5	T	T	-	5	1	1	T	1	T	T	T	T	T	62
	854.3	*10*	0.5	1.5	-	-	2.5	-	-	1	1	-	T	-	-	-	T	1	92
	949.4	*10*	T	1	T	25	-	-	5	17	2	-	-	-	-	-	-	1	49
6.4	1063.7	*10*	-	1	-	5	-	T	5	-	-	-	-	-	-	-	-	5	84
	1196.2	*10*	-	2	T	1	1	T	7.5	T	T	T	T	-	-	-	0.5	-	88
	1218.8	*10*	2	10	1	5	1	-	15	T	T	1	T	-	-	T	0.5	0.5	64
	1164.3	*2a+10*	0.5	5	1	1	2	-	5	1	1	1	T	-	-	-	T	-	82.5

al. 2005). Given that provenance is likely to change throughout a glacial cycle, the following discussion focuses on changes observed between selected LSUs and facies. Given the sampling resolution and the likely cyclic variation in provenance source indicators, identifying large-scale changes in provenance relative to depth is difficult to determine at this stage and will be assessed in greater detail at a later date.

Lithostratigraphic Unit 1 (0–82.74 metres below seafloor [mbsf])

LSU 1 consists of a series of truncated diamictites that are occasionally interbedded with thin conglomerate, sandstone and mudstone beds. The sandstone and mudstone beds (Facies 3) are dominated by feldspar, volcanic lithics, and volcanic glass. The diamictites and conglomerate units (Facies 7, 9, and 10) contain a distinct TAM provenance, with a notable presence (see Table 1) of rounded quartz (presumably from Devonian Beacon Supergroup sediments), metasedimentary rock fragments, dolerite, and granite. Mudstone and diamictite intraclasts, and deformation structures within the matrix, are observed in some of the diamictites (*e.g.*

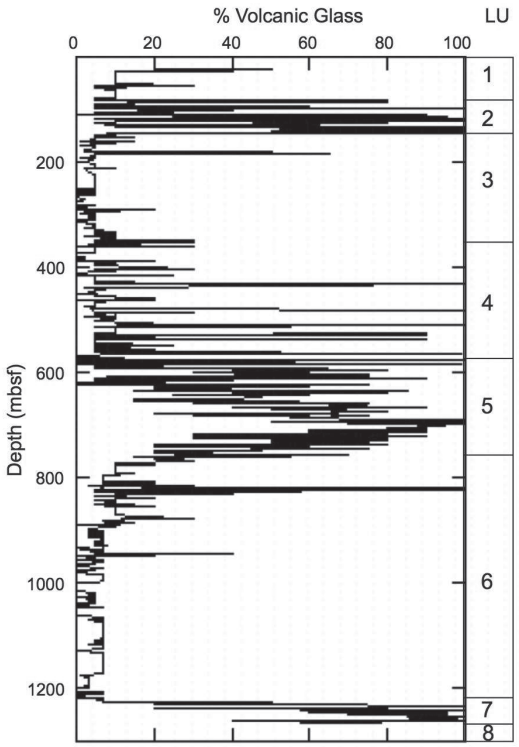

Fig. 1 – Chart showing variation in volcanic glass abundance with depth. Lithostratigraphic units (LSUs) are also shown.

26.68 mbsf; see Fig. 2). These intraclasts may be important indicators of deposition by grounded ice, and for identifying section of core where significant erosion of underlying mudstone/diamictite deposits has occurred.

Lithostratigraphic Unit 2 (82.74–146.79 mbsf)
Thin sections from this unit were not examined.

Lithostratigraphic Unit 3 (146.79–382.98 mbsf)
LSU 3 is characterised by interstratified diamictite and diatomite units. Within the diamictite facies (9 and 10) a shift in provenance from LSU 1 is apparent, with a general decrease in the abundance of rounded quartz (maximum of 2.5%), microcline, or plutonic rock fragments, suggesting less influence from the Beacon Supergroup, Ferrar Dolerites, or TAM granites. Volcanics and carbonates remain persistent throughout, but these also occur in LSU 1. Mudstone intraclasts are present in some thin sections, notably at 348.24 and 358.94 mbsf, where they dominate the assemblage. Microfabric structures are mostly obscured by the growth of carbonate cement within the matrix. Diagenetic carbonate is present in most diamictites, with some thin sections showing millimetre-scale variations between smectite-dominated and calcite-dominated matrix.

Lithostratigraphic Unit 4 (382.98–586.45 mbsf)
Thick diatomite units that are interstratifed with diamictite dominate LSU 4. The samples analysed were taken toward the base of the unit, and consist of stratified diamictite, mudstone with clasts, and sandstone. These units are notable by an increase in the degree of secondary calcite growth in the matrix. Well-sorted sandstone at 578.5 mbsf consists of angular quartz, feldspar, and opaque grains supported by authigenic carbonate cement.

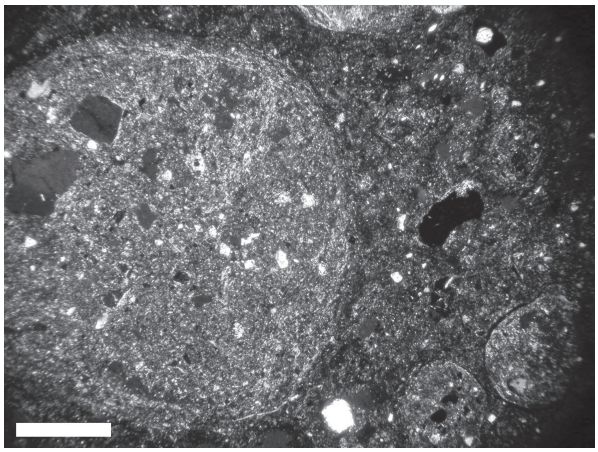

Fig. 2 – Mudstone and diamictite intraclasts within diamictite (26.68 mbsf). Scale bar is 500 µm.

Lithostratigraphic Unit 5 (586.45–759.32 mbsf)
LSU 5 consists of a volcanic-dominated series of interbedded sands and muds. Quartz is absent in a thin section taken from the upper sections of this unit; rather, the deposits are dominated by volcanic lithologies, probably locally derived. However, a thinly stratified diamictite towards the base of this unit at 750.8 mbsf showed significant amounts of angular and rounded quartz grains (see Fig. 3), although it lacks metasedimentary or plutonic clasts. Some laminae are composed almost entirely of quartz sand. The high abundance of quartz and lack of other TAM lithologies suggests a relatively restricted provenance and is currently interpreted to represent ice-rafted debris derived from TAM outlet glaciers. This sample indicates that some ice rafting was occurring during the onset of the volcanic activity that is inferred for LSU 5. Carbonate cement is also a characteristic of sediments within this unit.

Lithostratigraphic Unit 6 (759.32–1220.15 mbsf)
Lithostratigraphic Unit 6 is dominated by diamictite that is interbedded with mudstone and sandstone units. The diamictite is variable in composition, with rounded quartz, metasedimentary, and plutonic rock fragments present in some samples, but absent in others. The extent of carbonate cementation is also highly variable, with some samples dominated by calcite replacement of the clay matrix (*e.g.* at 1 009.4 and 1 063.7 mbsf), whereas a smectite-type clay matrix with minimal carbonate replacement dominates others. Mudstone intraclasts occur in some diamictites (*e.g.* 1164.3 mbsf).

CLAST PETROLOGY

Data were collected on the petrology and distribution of granule- to cobble-size clasts throughout the core. Preliminary results show significant downcore

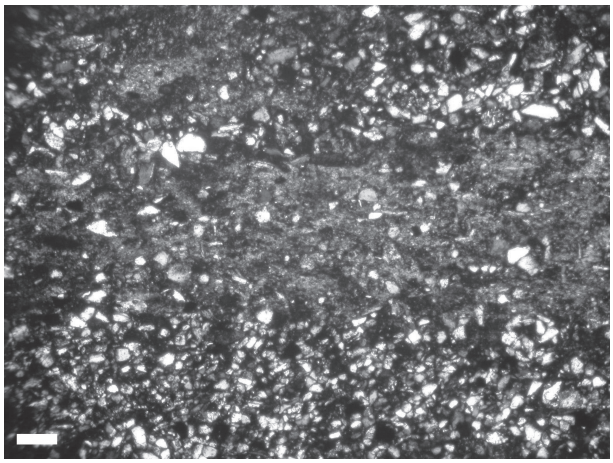

Fig. 3 – Stratified diamictite (750.8 mbsf) with quartz-dominated laminae. Outsized clasts are present in this unit and deform underlying laminae, suggesting an ice-rafted origin. Scale bar is 100 µm.

modal and compositional variations that provide direct information about the potential source regions and evidence of an evolving provenance, most likely as a result of changing ice-sheet conditions and ice-flow directions during deposition of sedimentary rocks recovered in the AND-1B drill core. In addition to the expected significant contribution from the 'local' McMurdo Volcanic Group, the dataset indicates a compositionally varied clast assemblage including several other rock types that are comparable to the dominant lithologies of more remotely located outcrops of the present-day TAM in Southern Victoria Land (SVL).

The following sections include: (i) a brief geological overview of the off-shore region with a particular focus on the pre-Cenozoic basement and cover rocks of the TAM in SVL and central TAM; (ii) a clast variability section, summarising the main downcore content and grain-size variations and clast distribution patterns; and (iii) a preliminary petrographical characterisation of all the sampled basement clasts and their downcore distribution, and the preliminary provenance inferences based on these petrographical descriptions. The term 'basement clast' is used here in a broad sense, to refer to the granule- to boulder-size clast population that was probably derived from the pre-Tertiary basement presently exposed in the TAM west and south of the AND-1B drill site.

Sampling, macroscopic observations, and preliminary petrographical analyses were performed following the same procedure and sample management adopted for the Cape Roberts Project (CRP)-1 core (Cape Roberts Science Team 1998c, 1998d), and analysis of the clast distribution followed the same procedure adopted in CRP-2/2A (Cape Roberts Science Team 1999).

DISTRIBUTION OF CLASTS AND MAIN LITHOLOGICAL TYPES

95 112 clasts were logged and counted on the basis of both lithology and particle size. The study also included sampling and thin-section examination of selected pebbles as needed during the logging phase to improve the characterisation of the main rock types. Total number of clasts per 1 m and per 10 centimetre (cm) intervals are presented in a graphical form using a logarithmic scale and integrated by means of PSICAT (Palaeontological Stratigraphic Interval and Construction Tool) in the lithological logs.

The total number of clasts per unit length shows major variations from 0 to 10 counts per metre for mud- or sand-rich intervals and in diatomite units (*e.g.* LSU 4.1), in the range c. 50-150 counts per metre for diamictite units (*e.g.* LSU 1.1, 6.1, 6.2) to very high values (up to 1 784) in some volcaniclastic intervals (*e.g.* at 639.33-640.33 mbsf in LSU 5.1, between 655.33 and 663.33 mbsf in LSU 5.3). Sharp variations across lithological boundaries are commonly present, as are fluctuations within units. Prominent downcore variations of the number of clasts were detected within the thick diamictite intervals in LSU 1.1, 6.1, and 6.2, consistently with the further subdivision of these thick units according to facies analysis (see Krissek et al. this volume).

Seven main lithological groups are distinguished. Their main features and clast dimensions can be summarised as follows:

1) Volcanic rocks. This group includes a variety of aphyric to porphyritic varieties, some vesicular and/or amygdale-bearing, ranging in composition from mafic to intermediate and felsic. All of these varieties mainly form granules to small- and medium-sized pebbles (see 'McMurdo Volcanic Rocks' section below for their detailed petrographical features and distributions throughout the core).
2) Granitoids. These consist mainly of biotite with or without hornblende granitoids (*e.g.* granites, syenogranites, and granodiorites) showing either isotropic fabrics or foliated to strongly mylonitic fabrics, with minor occurrence of deformed felsic porphyries and gabbroids; they are mostly represented within the pebble and small cobble class.
3) Metamorphic rocks. A variety of metamorphic rocks, ranging from basement rocks such as orthogneiss, paragneiss, and marble, to low-grade metasedimentary rocks of various origin (metalimestones, metagraywackes, metasandstones) are represented in this class (see 'McMurdo Volcanic Rocks' section). All of these rock types occur as granule, pebbles and cobbles.
4) Sedimentary rocks. These include at least two major lithological types: quartz-arenites and poorly to moderately sorted sandstones with granule-grade clasts (most likely reworked diamictites); these clasts mainly belong to the granule- and small-pebble classes.
5) Dolerites. These are generally fine- or medium-grained and with variable alteration, ranging from granule to subrounded pebbles and cobbles.
6) Quartz. It occurs as granules or small pebbles, some of them carrying minor micas, most likely interpreted as fragments of coarse-grained granitoids.

7) Intraclasts. Grey to black mudstones and minor sandstones were found to form the most common intraclast lithologies. Additional information on the distribution and composition of intraformational clasts is included in the legend of lithological logs. These clasts are generally represented within the granule and small pebble class. Although logged and described, these clasts will be omitted from quantitative provenance analysis but could be considered as a quantitative tool to investigate intrabasinal sediment recycling processes.

The detailed distribution of the different lithological types, combined with other logged features (shape, dimension) is the object of a quantitative provenance study, including the determination of relative proportions and of index values (*e.g.* the ratio: number of volcanic clasts/[number of volcanic clasts + number of basement clasts]), which can reliably show the evolving and different provenance of debris supplied to the drill site area from local, nearby volcanic centres and from more distal areas, presumably located in the TAM.

Both volcanic and granitoids are ubiquitous in most of the core, with volcanic rocks persistently forming the dominant lithology throughout the core a part from the diamictite units of LSU 1.1 (lower part) and some intervals of LSU 6.2 and LSU 8.1 where basement clasts of various compositions constitute the dominant component. In contrast, all other lithologies show a more restricted distribution. Based on semi-quantitative analyses of the dataset, the main distribution patterns can be summarised following the subdivision in LSUs as reported in table 2. Note that granitoid counts include quartz counts, assuming that most of quartz granules are derived from granitoids. Moreover, both intraformational clasts and sedimentary clasts were not considered. The latter can represent up to 35% of the clasts population in LSU 1.1, where sedimentary clasts are mainly clasts of reworked diamictite, but in most of the core they constitute a very minor component and are mainly represented by scattered small pebbles of quartz-arenites (most likely derived from the Beacon Supergroup). Further sampling and petrographical work will be necessary to better address the compositional and distribution pattern of this lithological group.

BASEMENT CLASTS AND PROVENANCE INFERENCES

As in previous drill cores (McMurdo Sound Sedimentary and Tectonic Studies [MSSTS]-1, Cenozoic Investigations in the western Ross Sea [CIROS]-1, CIROS-2, CRP-1, CRP-2/2A, CRP-3) on the western edge of the Victoria Land Basin (Hambrey et al. 1989; Cape Roberts Science Team 1998a, 1998d; Talarico & Sandroni 1998; Talarico et al. 1999; Sandroni & Talarico 2006), the AND-1B core provides clear evidence of a multi-component source for the supply of granule- to cobble-sized clasts to the Quaternary and Tertiary Cenozoic sedimentary sequences in the McMurdo Sound. The preliminary petrographical examination of basement clasts was performed following the same procedures and sample management adopted for CRP-1 and CRP-2/2A (Cape Roberts Science Team 1998b, 1998c, 1999).

Clast logging and preliminary sampling in AND-1B indicate that basement clasts are highly variable throughout the cored interval and that pebble- to

Tab. 2 - Lithostratigraphic units (LSU) and clast relative proportions among the main rock types in the uppermost 575 m of the MIS (AND-1B) drill core. Abbreviations are as follows: mbsf = metres below the sea floor; Vo = volcanic clasts; Bas = basement clasts (Gr = granitoid; Met = metamorphic; Dol = dolerite).

LSU	***Depth – top*** *(mbsf)*	***Depth – base*** *(mbsf)*	***Unit Thickness*** *(m)*	***Lithology***	***Estimated average clast proportions and basement clast compositions***
1.1	0.00	82.74	82.74	Muddy diamictite with mudstone and sandstone	Vo (10-90%) – Bas (90-10%) (Bas: Gr≈Met>>Dol)
2.1	82.74	86.63	3.89	Claystone and volcanic ash/tuff	Vo (ca. 100%)
2.2	86.63	94.52	7.89	Mudstone-rich diatomaceous ooze	Vo (100-70%) – Bas (0-30%) (Bas: Met >> Gr, rare Dol)
2.3	94.52	132.83	38.31	Diamictite, volcanic sandstone, and silty claystone	Vo (50-100) – Bas (50-0%) (Met≥Gr)
2.4	132.83	146.79	13.96	Volcanic sandstone, siltstone, and mudstone	Vo (> 95%) (Met 5%)
3.1	146.79	169.40	22.61	Muddy diamictite with diatomite	Vo (20-100%) – Bas (80-0%) (Met>>Gr)
3.2	169.40	181.93	12.53	Silty claystone and mudstone alternating with diatomite	Vo (100-50%) – Bas (0-50%) (Met>>Gr)
3.3	181.93	292.66	110.73	Alternating diamictite and diatomite	Vo (40-100%) – Bas (60-0%) (Met≥Gr, rare Dol)
3.4	292.66	347.19	54.53	Biosiliceous-bearing diamictite	Vo (≈ 85 %) – Bas (≈ 15%) (Met≥Gr, rare Dol)
3.5	347.19	363.37	16.18	Silty claystone, sandstone, and muddy diamictite	Vo (> 95%) (Met<5%)
3.6	363.37	382.98	19.61	Biosiliceous-rich diatomite, mudstone, and diamictite	Vo (55-100%) – Bas (45-0%) (Met≥Gr)
4.1	382.98	459.24	76.26	Diatomite	Vo (> 95%) (Met + Gr <5%) ; Vo 60% - Bas 40% (Met≥Gr) at ca. 454 mbsf
4.2	459.24	511.18	51.94	Diamictite, mudstone, and diatomite	Vo (70-100%) – Bas (30-0%) (Gr≥Met)
4.3	511.18	575.12	63.94	Volcanic diamictite, mudstone, and diatomite	Vo (50-100%) – Bas (50-0%) (Gr≥Met, rare Dol)

cobble-sized clasts consist of a significantly wider range of lithological types. The main lithological types can be grouped into five major groups: granitoids, metamorphic rocks, dolerites, quartz-arenites, and diamictite clasts.

A total of 182 samples, representative of all lithological types, were collected and are listed in table 3 (mineral abbreviations are according to Kretz 1983). Granitoid pebbles consist of dominant isotropic or foliated biotite granites and biotite-hornblende syenogranite and granodiorite. Minor lithologies include biotite-hornblende tonalite, isotropic or foliated biotite-hornblende quartz-diorite and gabbro, biotite-hornblende alkali feldspar granite, mylonitic or foliated muscovite-bearing granite, and felsic granitoids possibly derived by dyke swarms (*e.g.* microgranites, leucogranites, granophyres, mylonitic felsic porphyries). Preliminary microscopic examination revealed that all granitoid types show a variably developed alteration; allanite, zircon/monazite, apatite and titanite were found to be the most common accessory minerals. Most importantly, granitoid fabrics were found to be highly variable, including both isotropic, ipidiomorphic textures and variably foliated to mylonitic fabrics indicative of enhanced post-emplacement deformation.

The group of metamorphic clasts includes both rocks of felsic to mafic meta-igneous nature (*e.g.* mylonitic biotite with or without garnet orthogneiss, biotite granitic orthogneiss, metadiorites) and metasedimentary rocks derived from a wide range of protoliths and under a rather wide spectrum of metamorphic conditions. Orthogneisses, garnet-bearing biotite gneisses, amphibolites, and marble show mineral assemblages and microstructures consistent with upper amphibolite-facies (medium- to high-grade) regional metamorphic conditions. These clasts are particularly widespread in LSU 6.4 but some are found elsewhere, especially in a thin clast-rich interval at *c.* 454 mbsf (lower part of LSU 4.1) and in the core section below 511 mbsf (*e.g.* LSU 4.3). Biotitecalcite Ca-amphibole metasandstones, biotite slates/phyllites, metagraywackes, and metalimestones are characterised by decussate, spotted microstructures diagnostic of contact metamorphism, or more often by oriented fabrics indicative of syn-tectonic recrystallisations; in these rocks, mineral assemblages are indicative of biotite-zone (greenschist facies/low-grade) metamorphic conditions. The low-grade metasediments are scattered throughout the core, at places mixed only with foliated granitoids (*e.g.* LSU 1.1).

In conclusion, preliminary petrographical investigations indicate that several basement lithologies were involved as sources of basement clasts in the Cenozoic sedimentary strata recovered in the AND-1B drill core. As in CRP and CIROS cores (Talarico & Sandroni 1998; Talarico et al. 2000; Sandroni & Talarico 2001, 2004, 2006), the granitoid pebbles can be closely match to source-rock units belonging to the Cambro-Ordovician Granite Harbour Igneous

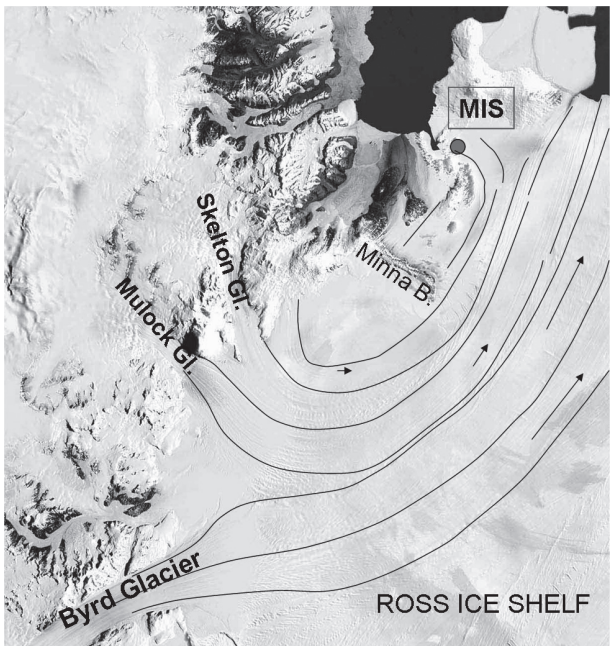

Fig. 4 – The region between Byrd and Skelton glaciers is identified as the potential source area for pebble- and cobble-size clasts as documented in several diamictite units (*e.g.* in LSU 6.4) and by some lonestones in AND-1B core.

Complex, which is the dominant component in the Ross Orogen in SVL (Gunn & Warren 1962; Allibone et al. 1993a, 1993b). The occurrence in AND-1B of pebbles of phyllites and low-grade metasandstones scattered throughout the core is noteworthy as the onshore exposures of these rocks are rather limited, and restricted to areas of the Skelton Group (Grindley & Warren 1964) between the Skelton and Mulock glaciers, about 100 kilometres (km) southwest of the AND-1B drill site.

Medium- to high-grade metamorphic rocks such as biotite-garnet gneiss, coarse-grained marble and orthogneiss are common rock types in the amphibolite facies Koettlitz Group between Koettlitz and Mackay glaciers (Grindley & Warren 1964; Williams et al. 1971; Findlay et al. 1984; Allibone 1992; Turnbull et al. 1994) but other medium- to high-grade metamorphic areas are exposed between the Darwin and Byrd glaciers and, farther south, in the upper Nimrod Glacier.

Based on the preliminary characterisation of low- to medium-grade metamorphic clasts and of foliated and mylonitic granitoids, the most likely source for these pebbles is the region between Skelton and upper Byrd glaciers (Fig. 4). Future off-ice investigations on the petrography and mineral chemistry in both metamorphic and plutonic pebbles and a detailed comparison with all the potentially similar offshore rock units in the Transantarctic Mountains will test and probably confirm these inferences on provenance.

McMURDO VOLCANIC ROCKS

Late Cenozoic alkali volcanic rocks of the McMurdo Volcanic Group (Kyle 1990) are widespread in the McMurdo Sound area (Fig. 5). These range in age

Tab. 3 - Preliminary petrographic description of basement clasts in AND-1B core.

Top (mbsf)	**Bottom** (mbsf)	**Classification**	**Top** (mbsf)	**Bottom** (mbsf)	**Classification**
19.79	19.80	Volcanic sandstone	368.66	368.67	Beacon quartz-arenite
28.32	28.34	Bt-Cal metasandstone	377.93	377.94	Metalimestone
28.60	28.61	Foliated Bt granite	381.21	381.23	Beacon quartz-arenite
30.45	30.48	Metalimestone	454.00	454.03	Hbl-Bt tonalite (slightly deformed)
35.71	35.73	Foliated Bt granite	454.12	454.15	Cpx-bearing Cam quartz-rich gneiss (mylonitic)
37.65	37.68	Brown Hbl quartz-monzonite (graphic texture)	454.98	455.00	Bt metasandstone (detrital Ms. neoblastic Bt)
42.93	42.96	Dolerite	461.74	461.77	Bt metasandstone
43.39	43.32	Dolerite	473.87	473.89	Ibrid sandstone (clasts: limestone. Qtz. Pl. Cal. Opm. Ms)
44.13	44.16	Cam-bearing Bt phyllite	518.53	518.57	Bt granite
44.40	44.43	Dolerite	519.44	519.46	Bt quartz-feldspatic gneiss
47.89	47.92	Dolerite	524.23	524.25	Dolerite
53.68	53.71	Dolerite	528.77	528.81	Mylonitic Bt granite
56.28	56.34	Ms-Bt-Pl calcite rich phyllite	534.93	534.95	Amphibolite
58.54	58.57	Diamictite clast including dolerite. granite. basalt. metasandstone clasts	535.52	535.53	Pl-bearing calc-schist
59.59	59.63	Hbl-Bt granodiorite	540.45	540.47	Mylonitic Ms granite
61.03	61.08	Bt-bearing quartz-rich metasandstone (microconglomerate) with cherts and claystone clasts	750.60	750.62	Bt phyllite. Bt-bearing metalime-stone. Bt metasandstone. Bt granite
61.84	61.88	Bt-bearing quartz-rich metasandstone (microconglomerate)	750.60	750.62	Dolerite
62.70	62.73	Altered Bt granite	750.79	750.80	Cal-Bt metasandstone
63.90	63.94	Foliated Hbl-Bt granodiorite	750.88	750.90	Bt quartzitic schist
64.45	64.49	Foliated Hbl-Bt granodiorite	750.91	750.92	Dolerite
69.64	69.69	Bt microgranite (Pl with Mc inclusions)	760.02	760.05	Bt metasandstone
72.44	72.47	Altered granophyric felsic (dyke)	760.18	760.22	Ms-Bt bearing feldspar-rich metasandstone
72.78	72.81	Porphyritic Bt granite (slightly deformed)	760.78	760.80	Bt syenogranite
72.86	72.89	Cam-Pl-Qtz phyllite	761.14	761.18	Layered Bt metasandstone
73.75	73.79	Bt microgranite (low M index; dyke?)	762.13	762.15	Bt metasandstone
76.35	76.38	Mudstone	761.92	761.93	Dolerite
78.55	78.57	Altered prophyric Bt granite (slightly deformed)	762.43	762.45	Chtd-bearing metalimestone. Qtz-Cpx-Pl granofels. Ms-bearing Bt phyllite
79.66	79.69	Foliated Bt granite	763.57	763.61	Foliated Bt granite
80.74	80.76	Porphyritic Bt granite (slightly deformed)	767.17	767.19	Foliated Bt granite
98.54	98.59	Bt metasandstone	767.77	767.79	Bt microgranite
101.84	101.88	Deformed felsic porphyry (or meta-microbreccia)	768.54	768.56	Bt syenogranite
106.11	106.14	Mylonitic felsic porphyry	772.36	772.39	Cal-Bt metasandstone
106.85	106.88	Bt-Ms quartz-feldspathic gneiss	778.70	778.73	Bt-bearing slate
124.49	124.50	Beacon quartz-arenite	791.14	791.16	Bt-bearing mylonitic porphyritic granite
124.49	124.52	Layered Bt-Pl-Czo/Ep phyllite	791.75	791.79	Bt-Hbl syenogranite
124.65		Bt metasandstone (decussate structure)	792.24	792.26	Bt metagraywacke
149.96	149.98	Ms-bearing Cal-rich phyllite	792.71	792.74	Mylonitic felsic porphyry or metaconglomerate
150.07	150.09	Bt-Sericite meta-microconglomerate	792.74	792.75	Mylonitic Bt granite
150.08	150.09	Hbl-Bt tonalite (Cpx relicts)	836.47	836.50	Foliated Bt-Hbl diorite
150.16	150.20	Cal-Bt phyllite	837.50	837.52	Cam-Pl schist
162.21	162.29	Cam-bearing Bt phyllites	853.51	853.53	Bt granitic orthogneiss
163.47	163.51	Bt microgranite (dyke?)	854.16	854.18	Qtz-rich Kfs mylonite
181.90	181.95	Bt metasandstone	854.41	854.43	Weakly foliated Bt-Hbl granodiorite
182.58	182.60	Mylonitic felsic porphyry	857.81	857.83	Bt-Hbl monzonite/granodiorite
188.21	188.22	Diamictite clasts with intermediate volcanics (mixed types) clasts and plagioclase lithics	858.12	858.13	Bt slate
242.16	242.21	Dolerite	883.80	883.82	Dolerite
249.97	249.99	Ms-Bt quartz-rich phyllite (Pl porphyroclasts)	894.02	894.04	Metalimestone
269.87	269.89	Claystone	899.88	899.91	Cam-Czo/Ep granofels
278.60	278.65	Hbl-Bt granodiorite	900.80	900.82	Metalimestone

Tab. 3 - Continued.

Top (mbsf)	Bottom (mbsf)	Classification	Top (mbsf)	Bottom (mbsf)	Classification
312.64	312.69	Bt syenogranite	901.95	901.97	Dolerite
344.03	344.05	Dolerite	905.01	905.02	Clasts: dolerite, polycrystalline quartz lithics
354.83	354.85	Hbl-Bt quartz-diorite	905.37	905.38	Bt microgranite
366.16	366.17	Granophyre (graphic texture, granitic compositon, dyke?)	910.14	910.16	Metalimestone
913.07	913.08	Clasts: volcanic of variable composition and texture	1126.00	1126.47	Bt-Cam phyllite with Cam-Pl layers
916.08	916.09	Cpx-Pl-Qtz very fine grained granofels	1133.03	1133.06	Mylonitic Bt granite/granitic orthogneiss
923.19	923.21	Cam-Cal-Pl layered metasandstone	1133.37	1133.39	Very fine grained Cpx-Pl granofels
936.53	936.54	Bt-Hbl quartz-diorite/tonalite	1139.46	1139.49	Cpx-Bt-Cam-bearing marble
937.12	937.15	Bt-Pl quartzite	1145.84	1145.86	Bt granitic orthogneiss
938.09	938.11	Hbl-Bt quartz-diorite	1150.82	1150.86	Bt-Cal phyllite
942.12	942.12	Bt metagraywacke with Qtz-rich domains	1157.60	1157.63	Weakly foliated Bt-bearing leucogranite (aplite)
942.47	942.48	Mylonitic Bt felsic porphyry or metaconglomerate	1167.82	1167.82	Bt-Hbl monzonite/granodiorite
943.70	943.73	Foliated Cam-Bt diorite	1167.91	1167.93	Bt-Hbl monzonite/granodiorite
943.85	943.86	Cam-bearing Bt plagiogneiss	1168.91	1168.93	Cpx-Pl fine grained granofels
944.09	944.10	Cam-Pl schist	1172.93	1172.96	Bt-Hbl granodiorite
949.47	949.00	Diamictite clast with metalimestone and felsic/intermediate volcanic clasts	1179.41	1179.44	Cpx-bearing plagioclase-rich gneiss
960.35	960.38	Bt-Hbl alkali-feldspar granite	1183.10	1183.13	Cpx-Pl-Scp gneiss with mylonitic Pl-Qtz layer (mylonitic migmatite)
961.44	961.46	Metamorphosed Bt-Cam microdiorite	1183.49	1183.53	Cpx-Ol (altered) marble
966.95	966.97	Contact metamorphosed Bt felsic porphyry	1184.03	1184.05	Bt granite
969.08	969.10	Bt granite	1186.38	1186.40	Foliated Bt-Hbl granodiorite
975.39	975.40	Phl-bearing marble	1187.51	1187.55	Cpx-Hbl gneiss and Bt-bearing granitic leucosome
979.19	979.20	Bt-Hbl quartz-diorite/gabbro	1189.63	1189.66	Cam-bearing Bt gneiss
985.86	985.88	Cal-bearing Cam-Bt schist	1190.80	1190.82	Leucogranite
988.63	988.65	Cam-Bt granitic orthogneiss	1195.70	1195.73	Cpx-Pl-Cam gneiss
1002.24	1002.25	Grt-bearing Bt migmatitic gneiss (tonalitic orthogneiss)	1199.89	1199.93	Bt-Cam schist
1004.48	1004.50	Foliated Bt-Hbl granodiorite	1200.90	1200.92	Bt quartzitic schist
1006.95	1006.96	Cam (Act)-bearing metabasalt	1203.07	1203.09	Layered Bt metasandstone
1009.33	1009.35	Czo/Ep-Qtz-Pl granofels	1204.44	1204.47	Bt microgranite
1015.04	1015.05	Foliated leucogranite or plagiogneiss	1205.83	1295.85	Ol (altered)-bearing marble
1068.37	1068.39	Dolerite	1207.94	1207.06	Bt-bearing mylonitic granite
1074.27	1074.28	Bt-Hbl diorite/gabbro	1213.56	1213.58	Foliated Bt-Hbl granodiorite
1076.59	1076.61	Bt-bearing metagraywacke	1213.79	1213.81	Bt-bearing foliated granite
1078.50	1078.54	Layered Cal-Bt metasandstone with Bt-phyllite layers and chert clasts	1214.01	1214.02	Bt-bearing foliated granite
1079.22	1079.24	Metalimestone	1217.41	1217.43	Bt-bearing amphibolite with Cpx relics
1080.57	1080.59	Clasts: felsic volcanic, Bt metasand-stone, Ms-bearing slate/phyllite, marble	1219.65	1219.67	Cpx-Phl-bearing marble
1094.79	1094.81	Bt-Cal metasandstone	1229.68	1229.70	Cal metasandstone
1095.02	1095.03	Bt metagraywacke/slate	1279.74	1279.77	Cpx-Phl gneiss
1095.58	1095.63	Bt metagraywacke/slate	1279.79	1279.81	Altered Bt-Cam gabbroid
1103.51	1103.53	Contact metamorphosed Bt metagraywacke	1280.04	1280.08	Foliated Ms-Bt granite
1104.08	1104.12	Foliated leucogranite or plagiogneiss	1282.22	1282.24	Bt granite
1124.82	1124.85	Bt gneiss	1283.87	1283.89	Grt-bearing Bt orthogneiss
1125.72	1125.76	Mylonitic Bt-Hbl granodiorite			

over 19 m.y. from the currently active Erebus volcano to a subvolcanic peralkaline trachyte dike complex at Mount Morning, to the southwest of the drill site (Kyle 1990 & references therein). A thick pumice lapilli tuff, dated at 22 Ma, was found in the Cape Roberts Project cores (Armienti et al. 2001, McIntosh 2001). Eruptive vents on Ross, White, and Black islands surround the MIS drill site. Aeromagnetic studies have also suggested the possibly of submarine volcanoes beneath the McMurdo Ice Shelf. Minna Bluff to the south of the drill site formed between 7 and 11 Ma and has acted as an important barrier to the flow of the Ross Ice Shelf into McMurdo Sound (Kyle 1981). There is a major glacial unconformity dated between 10 and 11 Ma on Minna Bluff and it is interpreted as a result of erosion by an early Ross Ice Sheet. It

was therefore expected that clasts from the Minna Bluff area would be common and important in glacial deposits in the MIS cores.

An objective of the drilling at MIS was to obtain a better understanding of the volcanic record in the southern Ross Sea and to examine the relationship between volcanism and glacial dynamics.It has been proposed that Erebus volcano overlies a mantle plume or hot spot and if so this would have implications to rifting within the Ross Sea. Therefore, an understanding of the nature and tempo of volcanism also provides insights into an understanding of tectonic processes. Perhaps the most important role of volcanism was to provide volcanic material that could be radiometrically dated (*e.g.* $^{40}Ar/^{39}Ar$ dating) and thus provide time planes within the core. Chronology is always critical in drill cores and it was thought that the location of the MIS hole so close to many volcanic vents would allow for the development of a well-calibrated time scale.

NOMENCLATURE

Volcanic rocks are usually classified based on their chemical composition because they are usually glassy or have fine-grained groundmass that does not allow the mineralogical composition to be determined. The total alkali-silica (TAS) diagram has been adopted recently by the international community to classify volcanic rocks (Le Maitre 2002). Geological and geochemical studies have shown the lavas in McMurdo Sound area define several major fractionation lineages. Since about 10Ma the lavas have mostly belonged to one of several basanite-phonotephrite-tephriphonolite-phonolite lava lineages and prior to 10 Ma their compositions were usually less undersaturated and part of an alkali basalt-trachyte association (*e.g.* alkali basalt-hawaiite-mugearite-benmoreite-trachyte).

A simple classification was used for characterising volcanic materials in the core based on the mineral assemblage recognisable in thin sections:

Mafic (basaltic): characterised by phenocrystic olivine and clinopyroxene with or without plagioclase in the groundmass.

Intermediate: phenocrysts of plagioclase ± kaersutite ± clinopyroxene

Felsic (phonolitic, trachytic): phenocrysts of K-feldspar ± kaersutite ± sodic clinopyroxene (acmite).

Volcanic glass compositions, from selected intervals, were classified with a TAS diagram (Fig. 6).

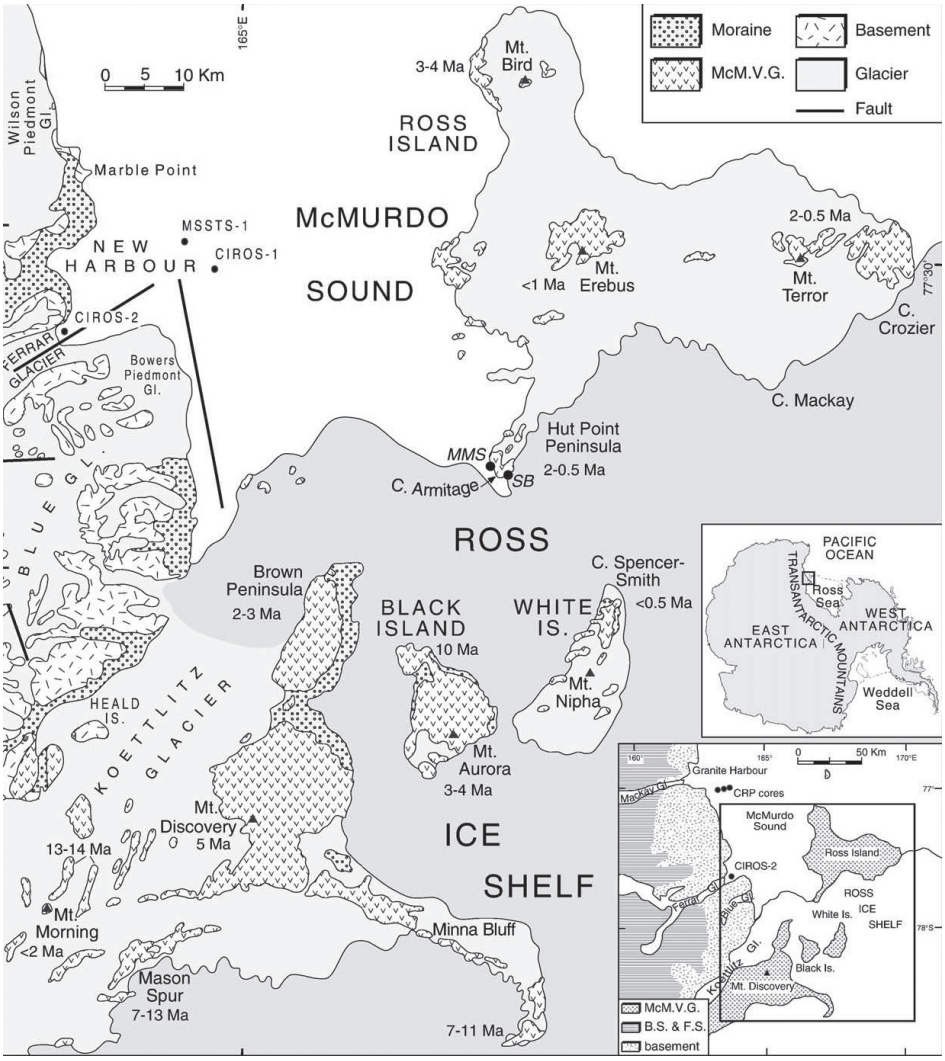

Fig. 5 – Geological map of the southwest corner of the Ross Sea (redrawn from Sandroni & Talarico, 2006) showing McMurdo Volcanic Group exposures and generalised ages for the major volcanic centres within the Erebus Volcanic Province (Kyle, 1990). Inset map represents a geological sketch of the McMurdo Sound area (simplified after Warren, 1969), showing basement complex, cover complex (Beacon and Ferrar supergroups) and McMurdo Volcanic Group outcrop areas. Locations of MSSTS-1, CIROS-1, CIROS-2, and CRP drill sites are also shown. Abbreviations are: B.S. = Beacon Supergroup; F.S. = Ferrar Supergroup; McM. V.G. = McMurdo Volcanic Group; Gl. = Glacier; Is. = Island; C. = Cape; MMS = McMurdo Station; SB = Scott Base.

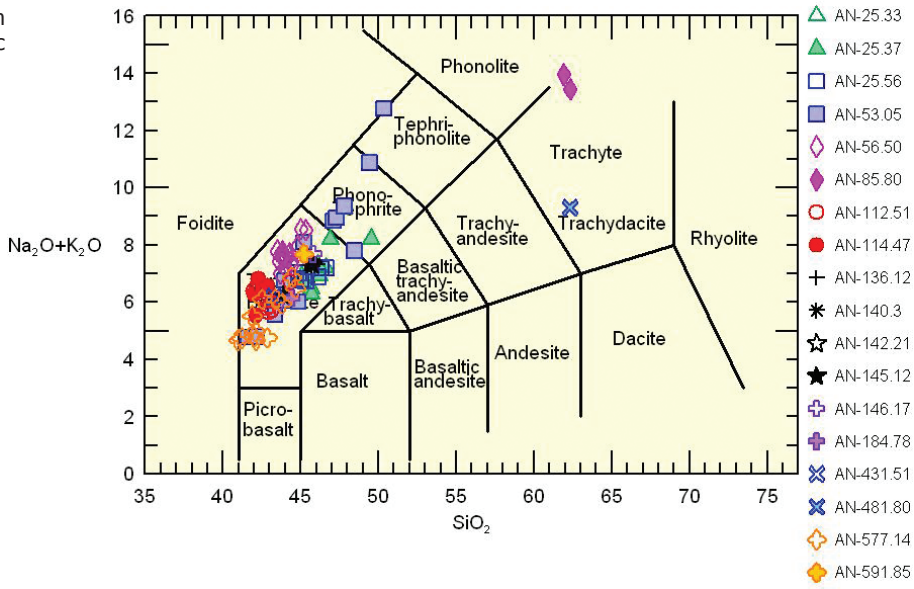

Fig. 6 – Total alkali-silica (TAS) diagram (Le Maitre, 2002) for selected volcanic glass compositions in AND-1B.

DISTRIBUTION AND PETROLOGY OF VOLCANIC ROCKS

Volcanic rocks occur in the core in a variety of lithologic units: as clasts in poorly sorted sedimentary rocks (diamictite, mudstone with clasts, breccia, conglomerate), as constituents in well-sorted units (sandstone, mudstone), and as primary volcanic deposits (lava, lapilli tuff, tuff). Volcanic clasts comprise approximately 70% of the total clast count (total number = 95 112, see 'Distribution of Clasts and Main Lithological Types' section above). The 'volcanic' modifier is applied to all units that contain >50% volcanic material, as identified through smear slides. Most of the 'volcanic' sediments are characterised as resedimented volcanic rocks although a number of primary tephra fall deposits do occur. The degree of reworking is variable and some units are interpreted to be 'near-primary' deposits. The designation of near-primary is based on the lithologic homogeneity and textural characteristics (sorting, rounding, clast shape, *etc.*) of the unit. The occurrences of volcanic rocks in the AND-1B core are described in the context of eight lithostratigraphic units (LSU 1-8) defined by the ANDRILL MIS sedimentology team. The core description phase included on-ice logging of volcanic layers and petrographic characterisation of selected thin sections (see details in Tab. 4), and post-ice electron microprobe (EMP) analysis of volcanic glass from selected intervals.

Lithostratigraphic Subunit 1.1 (0–82.74 mbsf)

Volcanic sediment, including well-sorted siltstone to sandstone, occur in the upper interval (<26.43 mbsf) and throughout the whole LSU. These volcanic sediments tend to be horizontally well stratified and are composed of fresh brown glassy lapilli and ash shards. The glass shows a large range in vesiculation and the shape varies from very angular to subrounded (Fig. 7a, 7b). The only recognisable phenocrysts are (>1 mm) mafic minerals. However, fragments of mafic minerals also occur in the sediment. In the very shallow layers (above *c.* 10 mbsf, sampled with core catchers), glass shards are very angular and show jigsaw textures. Volcanic pebbles in the core catcher are pieces of a hyaloclastite breccia, formed by fragments of felsic rocks with large feldspar characterised by a jigsaw fracture pattern that is cemented by calcite. Volcanic granules and pebbles dispersed within diamictites show a large compositional variation ranging from porphyritic mafic rocks with large olivine phenocrysts to felsic rocks with trachytic texture. Glass has as large compositional variability ranging basanite to tephriphonolite (Fig. 6). More evolved compositions (up to tephriphonolite) appear concentrated in the upper part of the LSU (<50 mbsf).

Lithostratigraphic Subunit 2.1 (82.74–86.63 mbsf)

In this interval, McMurdo volcanics form lapilli-tuff, tuff and volcanic sand deposits. The thickest and the best-preserved lapilli-tuff bed (85.27 to 85.87 mbsf) is made by angular, occasionally fluidal-shaped, tube pumices (Fig. 7c). The pumice clasts show a fresh light phonolitic glass (Fig. 6) and contain few feldspar microlites. For this reason we classified these rocks as felsic. Black lithic clasts and euhedral feldspars crystals also occur in these deposits. Ash and volcanic sands are mainly composed of a mix of angular felsic pumices and brown (probably mafic) glassy and vesiculated clasts.

Lithostratigraphic Subunit 2.2 (86.63–94.52 mbsf)

McMurdo volcanics form intermediate to felsic pebbles, whereas grains in diamictites are vesiculated, brown (mafic) glassy shards.

Lithostratigraphic Subunit 2.3 (94.52–132.83 mbsf)

In this interval, McMurdo volcanics comprise pebble clasts mainly felsic in composition in diamictites. Volcanic sandstones are made of vesiculated, fluidal, or angular ash grains (Fig. 7d). These shards contain few olivine and clinopyroxene microphenocrysts set in a brown fresh glass. Glass compositions fall into the tephrite-basanite field of TAS (Fig. 6).

Tab. 4 - Preliminary petrographic description of McMurdo volcanics in AND-1B core.

LSU	Top	Bottom	Rock Type	Composition on the basis of petrography	Notes
1.1	9.99	10.08	Hyaloclastite breccia	Felsic	Clast with large >5 mm feldspar clasts, carbonate cements
1.1	10.08	13.12	Volcanic clast	Intermediate	Large (>1 cm) phenocrists of feldspar
1.1	10.08	13.12	Volcanic Sandstone	Clasts with different compositions	Brown glassy vesiculated clasts, matrix supported
1.1	10.08	13.12	Volcanic Sandstone	Clasts with different compositions	Brown glassy non vesiculated clasts with jigsaw and hydration cracks, crystals, kaersutite
1.1	13.10	15.84	Hyaloclastite breccia	Clasts with different compositions (mainly intermediate)	Clast with large >5 mm feldspar clasts, jigsaw
1.1	13.12	15.84	Hyaloclastite breccia	Clasts with different compositions (mainly intermediate)	Clast with large >5 mm feldspar clasts, jigsaw
1.1	19.73	19.73	Volcanic Mudstone		Altered
1.1	19.77	19.77	Volcanic Mudstone		Altered
1.1	19.79	19.80	Volcanic Sandstone		
1.1	19.87	19.87	Volcanic Mudstone		Mainly crystal
1.1	19.98	19.98	Volcanic Mudstone		Rare glassy shards
1.1	20.11	20.15	Volcanic clast	Intermediate	
1.1	24.28	24.30	Volcanic Sandstone	Clasts with different compositions	Glassy brown angular lapilli and grains
1.1	25.05	25.06	Volcanic Sandstone	Clasts with different compositions	Glassy vesiculated brown clasts
1.1	25.24	25.27	Volcanic Sandstone	Clasts with different compositions	Glassy brown vesiculated lapilli and grains
1.1	25.29	25.30	Volcanic Sandstone	Clasts with different compositions	Glassy brown vesiculated angular lapilli and grains
1.1	25.45	25.50	Volcanic Sandstone	Clasts with different compositions	Glassy brown vesiculated angular lapilli and grains
1.1	25.63	25.64	Volcanic Sandstone	Clasts with different compositions (mainly mafic)	Glassy brown vesiculated subangular lapilli and grains, mafic crystals
1.1	25.73	25.74	Volcanic Sandstone	Clasts with different compositions	Brown glassy angular grains
1.1	25.95	25.96	Volcanic Sandstone	Clasts with different compositions (mainly mafic)	Brown glassy vesiculated and subrounded lapilli and grains, mafic crystals
1.1	26.08	26.09	Volcanic Mudstone		Bad Thin section
1.1	26.15	26.16	Volcanic Sandstone	Clasts with different compositions (mainly mafic)	Brown glassy vesiculated and subrounded lapilli and grains, mafic crystals
1.1	27.76	27.78	Volcanic clast	Felsic	
1.1	28.03	28.11	Volcanic clast	Felsic	
1.1	30.52	30.54	Diamictite	Clasts with different compositions (mainly intermediate)	
1.1	30.74	30.77	Diamictite	Clasts with different compositions (mainly intermediate)	A mafic clast with large olivine phenocrysts
1.1	31.49	31.50	Volcanic clast	Mafic	Large olivine phenocrysts
1.1	32.15	32.19	Volcanic Sandstone	Clasts with different compositions	Calcite cement, Kaersutite crystals
1.1	32.24	32.25	Volcanic clast	Mafic	Palagonitised clast, with large olivine and calcite and filling of vesicles
1.1	32.63	32.65	Diamictite	Clasts with different compositions (mainly intermediate-felsic)	Glassy clast
1.1	33.53	33.55	Diamictite	Clasts with different compositions	Crystal rich
1.1	34.52	34.53	Diamictite	Clasts with different compositions	Some pumiceous clasts. Crystals
1.1	34.53	34.54	Diamictite	Clasts with different compositions	Some pumiceous glassy clast. Crystals
1.1	35.25	35.26	Volcanic clast	Intermediate	Glassy and kaersutite rich
1.1	35.53	35.64	Volcanic clast	Felsic	
1.1	35.83	35.86	Diamictite	Clasts with different compositions (mainly mafic)	Mainly glassy brown vesiculated subangular lapilli and grains, mafic crystals
1.1	35.94	35.98	Diamictite	Clasts with different compositions	Bad Thin section
1.1	36.87	36.91	Diamictite	Clasts with different compositions (mainly intermediate)	Some pumiceous clasts. Crystals
1.1	37.36	37.38	Diamictite	Clasts with different compositions	Altered clasts
1.1	37.40	37.45	Volcanic clast	Mafic	
1.1	37.98	38.00	Diamictite	Clasts with different compositions (mainly intermediate)	Only few volcanics
1.1	38.95	38.98	Diamictite	Clasts with different compositions (mainly intermediate-felsic)	Some altered pumice
1.1	39.83	39.86	Diamictite	Clasts with different compositions (mainly intermediate-felsic)	Some altered pumice
1.1	41.09	41.12	Diamictite	Clasts with different compositions (mainly intermediate)	Some pumice and golden glassy clasts
1.1	41.19	41.22	Diamictite	Clasts with different compositions	Abundant non volcanic clasts
1.1	43.50	43.52	Volcanic clast	Intermediate	
1.1	43.99	44.02	Diamictite	Clasts with different compositions (mainly mafic)	Glassy golden and vesiculated subrounded lapilli and grains, mafic crystals
1.1	44.96	44.99	Volcanic clast	Intermediate	
1.1	45.04	45.06	Diamictite	Clasts with different compositions	
1.1	45.28	45.31	Diamictite	Clasts with different compositions	Contains clasts of glassy tuff
1.1	52.61	52.71	Volcanic Breccia	Felsic	Calcite cement, Glassy clasts are palagonitised
1.1	52.61		Volcanic clast	Mafic	
1.1	52.61	52.71	Volcanic clast	Felsic	Large amphibole
1.1	52.90	52.94	Volcanic clast	Mafic	
1.1	53.06	53.07	Volcanic Sand	Clasts with different compositions	Some angular non vesiculated golden glassy shards
1.1	56.50	56.51	Volcanic Sand	Clasts with different compositions (mainly mafic-intermediate)	Some pumiceous golden glassy clast. Crystals
1.1	57.40	57.42	Mudstone		Mainly crystal fragments
1.1	58.54	58.57	Diamictite	Clasts with different compositions	Few altered volcanic clasts
1.1	58.82	58.84	Volcanic clast	Mafic	Large olivine phenocrysts
1.1	64.73	64.75	Volcanic clast	Intermediate	
1.1	65.06	65.08	Diamictite	Clasts with different compositions	Mostly non volcanic, abundant basement crystals
1.1	66.63	66.67	Volcanic clast	Felsic	
1.1	66.88	66.91	Diamictite	Clasts with different compositions	Mostly non volcanic, abundant basement crystals
1.1	68.89	68.91	Volcanic clast	Felsic	Deeply altered
1.1	72.19	72.21	Diamictite	Clasts with different compositions	Mostly non volcanic, abundant basement crystals

Tab. 4 - Continued.

LSU	Top	Bottom	Rock Type	Composition on the basis of petrography	Notes
1.1	74.42	74.47	Diamictite	Clasts with different compositions	Rare altered pumices
1.1	75.20		Diamictite	Clasts with different compositions	Traction texture, few volcanics
1.1	76.35	76.38	Mudstone		
1.1	79.19	79.23	Volcanic clast	Felsic	
1.1	80.46	80.50	Volcanic clast	Felsic	Altered
1.1	81.76	81.77	Volcanic clast	Felsic	Altered pumices
2.1	82.78	82.81	Diamictite		
2.1	83,00	83.02	Volcanic Sand		Pumices and brown glassy clasts
2.1	83.34	83.36	Volcanic Sand	Felsic	Pumices
2.1	83.63	83.65	Volcanic clast	Felsic	
2.1	83.87	83.9	Volcanic Sand	Mix Pumice+mafic glass	
2.1	84.10	84.14	Volcanic Sand	Mix Pumice+mafic glass	
2.1	85.39	85.41	Volcanic Sand		Pumices
2.1	86.19		Volcanic Mudstone		
2.1	86.33	86.36	Diamictite		Pumices and brown glassy clasts
2.1	86.36	86.39	Diamictite		
2.1	86.39	86.42	Volcanic Mudstone		Pumices
2.2	92.27	92.28	Volcanic Sand		
2.2	92.76	92.80	Volcanic clast	Intermediate	
2.2	92.90	92.92	Volcanic clast	Felsic	
2.2	93.74	93.76	Diamictite	Mafic	Mafic glasses
2.3	96.21	96.24	Volcanic clast	Felsic	
2.3	97.09	97.12	Volcanic Mudstone		
2.3	100.01	100.03	Volcanic clast	Felsic	
2.3	100.09	100.10	Diamictite		
2.3	100.71	100.74	Volcanic clast	Felsic	Vesiculated glass
2.3	101.28	101.30	Volcanic clast	Felsic	
2.3	103.16	103.19	Volcanic Sand	Mafic	
2.3	103.79	103.81	Volcanic clast	Felsic	
2.3	104.90	104.92	Volcanic clast	Felsic	
2.3	107.13	107.16	Diamictite		Intraclasts
2.3	109.32	109.32	Volcanic Sand	Mafic	
2.3	110.87	110.88	Volcanic Sand	Mafic	Kaersutite
2.3	110.88	110.89	Volcanic Sand	Mafic	
2.3	112.07	112.07	Volcanic Sand	Mafic	
2.3	113.84	113.85	Volcanic Sand	Mafic	
2.3	114.94	114.95	Volcanic Sand	Mafic	Fluidal shape clasts
2.3	117.13	117.16	Volcanic Sand	Mafic	Kaersutite
2.3	117.53	117.54	Volcanic clast	Felsic	Abundant Kaersitite
2.3	118.10	118.11	Volcanic clast	Felsic	
2.3	118.82	118.83	Volcanic Sand	Mafic	
2.3	119.23	119.24	Volcanic Sand	Mafic	
2.3	119.65	119.66	Volcanic Sand		
2.3	120.09	120.10	Volcanic Sand		
2.3	120.88	120.89	Volcanic Sand		
2.3	123.29	123.30	Volcanic clast	Intermediate	
2.3	124.59	124.62	Volcanic clast	Felsic	
2.3	124.59	124.62	Volcanic clast		
2.3	126.17	126.20	Volcanic clast	Intermediate	
2.3	126.38	126.41	Volcanic clast	Felsic	
2.3	128.54	128.58	Diamictite		
2.3	130.78	130.79	Volcanic Mudstone		
2.3	131.77	131.78	Volcanic Mudstone		
2.4	133.35	133.37	Volcanic Mudstone		
2.4	134.51	134.53	Diamictite		
2.4	134.72	134.75	Volcanic clast	Intermediate	
2.4	134.73	134.74	Diamictite	Intermediate	
2.4	135.06	135.07	Volcanic Sand	Intermediate	
2.4	135.94	135.96	Volcanic Sand	Intermediate	Coarse and vesicular clasts
2.4	137.15	137.16	Volcanic Sand	Intermediate	Coarse and vesicular clasts
2.4	137.92	137.94	Volcanic Sand	Intermediate	Coarse and vesicular clasts
2.4	139.08	139.16	Volcanic Sand		
2.4	139.39	139.41	Volcanic Sand	Intermediate	
2.4	140.39	140.41	Volcanic Sand	Intermediate	Plagioclase
2.4	141.62	141.65	Volcanic Sand	Intermediate	
2.4	142.34	142.36	Volcanic Sand	Intermediate	
2.4	142.75	142.77	Volcanic Sand	Intermediate	Coarse
2.4	143.21	143.23	Volcanic Sand	Intermediate	
2.4	143.33	143.50	Volcanic Sand		
2.4	143.90	143.92	Volcanic Mudstone	Intermediate	
2.4	144.54	144.55	Volcanic Mudstone		
2.4	145.31	145.32	Volcanic Mudstone		
2.4	146.39	146.40	Volcanic Mudstone		
2.4	146.76	146.77	Volcanic Sand		
3.1	148.12	148.14	Volcanic clast	Mafic	Glassy (pillow ?) rim, olivine rich
3.1	148.41	148.43	Volcanic Sand	Clasts with different compositions (mainly mafic)	Glassy golden subangular shards
3.1	149.07	149.10	Volcanic clast	Intermediate	
3.1	154.48	154.49	Volcanic clast	Intermediate	Secondary silica minerals and pyrite filling of vesicles
3.1	156.19	156.20	Volcanic clast	Intermediate	
3.1	159.31	159.35	Volcanic Mudstone		Very rare glassy shards, kaersutite
3.1	162.13	162.15	Volcanic clast	Intermediate	
3.1	163.37	163.40	Volcanic clast	Intermediate	Secondary calcite filling of vesicles
3.1	163.76	163.78	Volcanic clast	Felsic	Large Sanidine rare Acmite phenocryst, Calcite filling of vesicles and veins

Tab. 4 - Continued.

LSU	Top	Bottom	Rock Type	Composition on the basis of petrography	Notes
3.1	163.90	163.93	Volcanic clast	Intermediate	Large plagioclase, Calcite filling of vesicles
3.1	164.63	164.65	Volcanic clast	Felsic	
3.2	173.72	173.75	Volcanic clast	Mafic	Large mafic crystals
3.2	177.95	177.97	Volcanic clast	Mafic	
3.2	178.36	178.29	Volcanic clast	Felsic	
3.2	178.46	178.49	Volcanic clast	Intermediate	
3.2	178.73	178.75	Volcanic Mudstone		barely recognisable glass shards
3.3	182.11	182.21	Volcanic clast	Intermediate	Calcite filling of vesicles, Kaersutite
3.3	182.51	182.52	Volcanic clast	Intermediate	Kaersutite breakdown products
3.3	182.53	182.56	Volcanic clast	Felsic	
3.3	182.60	182.61	Volcanic clast	Felsic	Strongly altered
3.3	182.69	182.71	Volcanic ??clast		
3.3	182.91	182.92	Volcanic clast	Felsic	Strongly altered
3.3	184.83	184.84	Mudstone		No recognisable igneous material
3.3	185.23	185.27	Volcanic clast	Intermediate	Kaersutite rich, Zeolite filling of vescicles
3.3	187.28	187.31	Volcanic clast	Felsic	Glassy groundmass, Kaersutite, remnants of large mafic and feldspar crystals
3.3	187.91	187.96	Volcanic clast	Mafic	
3.3	188.21	188.22	Diamictite	Clasts with different compositions (mainly felsic)	Some altered pumice clasts. Crystals. Secondary calcite filling of bubbles and veins
3.3	189.47	189.49	Diamictite	Clasts with different compositions (mainly felsic)	Some altered pumice clasts. Crystals. Secondary calcite filling of bubbles and veins.
3.3	192.70	192.72	Sandy mudstone	Clasts with different compositions (mainly mafic-intermediate)	Glassy subangular shards
3.3	193.74	193.76	Volcanic clast	Felsic	Altered. Some large feldspar
3.3	193.75	193.78	Volcanic clast	Felsic	Some large feldspar
3.3	202.05	202.07	Volcanic clast	Mafic	Some large mafic crystals, Secondary calcite filling of bubbles and veins
3.3	203.44	203.48	Volcanic clast	Intermediate	Secondary calcite filling of bubbles and veins
3.3	204.67	204.70	Volcanic clast	Mafic	Some large mafic crystals, Secondary calcite filling of vesicles and veins
3.3	204.75	204.79	Volcanic clast	Felsic	
3.3	205.79	205.80	Volcanic clast	Felsic	
3.3	205.93	205.95	Volcanic clast	Mafic	
3.3	207.24	207.28	Volcanic clast	Mafic	Some large mafic crystal
3.3	208.29		Volcanic clast	Mafic	Kaersutite
3.3	208.29	208.33	Volcanic clast	Mafic	Large mafic crystals altered
3.3	208.84	208.85	Volcanic clast	Mafic	Large mafic crystals
3.3	221.58		Volcanic clast	Mafic	Kaersutite
3.3	222.69	222.72	Volcanic clast	Intermediate	Strongly pyritised
3.3	226.48	226.5	Volcanic clast	Felsic	
3.3	228.18	228.2	Volcanic clast	Mafic	
3.3	228.22	228.24	Volcanic clast	Felsic	Secondary silica mineral filling of vesicles
3.3	228.67	228.69	Volcanic clast	Mafic	
3.3	229.10	229.14	Volcanic clast	Felsic	
3.3	230.65	230.70	Volcanic clast	Felsic	
3.3	237.3	237.31	Volcanic clast	Mafic	Glassy, alteration rim, secondary calcite filling of vesicles and veins
3.3	237.79	237.82	Volcanic clast	Felsic	
3.3	238.41	238.44	Volcanic clast	Mafic	Secondary calcite replaces olivine
3.3	238.90	238.92	Volcanic clast	Mafic	Secondary calcite filling of vesicles and veins and replaces olivine
3.3	240.49		Volcanic clast	Mafic	
3.3	241.67	241.71	Diamictite	Clasts with different compositions (mainly mafic)	Several non volcanic clasts
3.3	248.08	248.12	Diamictite		
3.3	257.16	257.20	Volcanic clast	Mafic	
3.3	260.58	260.60	Diamictite	Clasts with different compositions	Abundant subrounded brown glassy clasts.
3.3	260.73	260.79	Volcanic clast	Mafic	Secondary calcite replaces olivine
3.3	262.49	262.53	Volcanic clast	Mafic	Secondary calcite replaces olivine
3.3	266.83	266.85	Volcanic clast	Mafic	Secondary calcite replaces olivine
3.3	269.87	269.89	Diamictite		No volcanic clasts, only occasional crystals
3.3	275.42	275.45	Mudstone		
3.3	275.77	275.81	Volcanic clast	Mafic	
3.3	278.14	278.16	Diamictite	Clasts with different compositions (mainly mafic)	Very rare glassy shards
3.3	278.28	278.34	Volcanic clast	Mafic	
3.3	278.32	278.35	Volcanic clast	Mafic	
3.3	280.64	280.66	Volcanic clast	Mafic	
3.3	280.77	280.8	Volcanic clast	Mafic	
3.3	280.98	281.05	Volcanic clast	Felsic	
3.3	290.21	290.25	Sandy mudstone	Clasts with different compositions (mainly intermediate)	
3.3	291.55	291.56	Mudstone		
3.3	291.87	291.89	Volcanic clast	Mafic	
3.4	295.53	295.58	Volcanic clast	Mafic	
3.4	295.65	295.68	Volcanic clast	Felsic	
3.4	295.83	295.84	Volcanic clast	Felsic	Red oxidised groundmass
3.4	295.86	295.88	Diamictite	Clasts with different compositions (mainly felsic)	Some pumiceous clasts. Crystals
3.4	296.43	296.44	Volcanic clast	Mafic	Secondary calcite replaces olivine
3.4	296.93	296.96	Volcanic clast	Felsic	
3.4	297.06	297.12	Volcanic clast	Mafic	Picritic

Tab. 4 - Continued.

LSU	Top	Bottom	Rock Type	Composition on the basis of petrography	Notes
3.4	300.75	300.77	Volcanic clast	Mafic	
3.4	301.56	301.68	Volcanic clast	Felsic	Pumiceous clast
3.4	301.97	301.99	Volcanic clast	Mafic	
3.4	306.89	306.93	Volcanic clast	Intermediate	
3.4	319.78	319.81	Diamictite	Clasts with different compositions (mainly intermediate)	Glassy pumiceous clasts, Crystals
3.4	323.41	323.46	Volcanic clast	Mafic	
3.4	323.90	323.91	Volcanic clast	Felsic	
3.4	326.35	326.37	Volcanic clast	Mafic	
3.4	332.28	332.31	Diamictite	Clasts with different compositions (mainly mafic)	Crystals. Rare glassy shards
3.4	333.11	333.16	Volcanic clast	Felsic	
3.4	335.81	335.82	Volcanic clast	Felsic	Large Feldspar
3.4	336.72	336.74	Diamictite	Felsic	Large felsic altered single clast, Crystals, Rare glassy clasts
3.4	341.10	341.14	Volcanic clast	Mafic	
3.4	344.67	344.70	Diamictite	Clasts with different compositions (mainly intermediate-felsic)	Crystals. Rare glassy shards
3.5	348.03	348.04	Diamictite	Clasts with different compositions (mainly intermediate)	Brown glassy vesiculated granules, crystals, Kaersutite
3.5	349.63	349.64	Diamictite	Clasts with different compositions	Very heterogenous, felsic clasts, tube pumices, brown shards, crystals (acmite, kaersutite)
3.5	352.83	352.86	Volcanic clast	Mafic	
3.6	363.94	363.97	Volcanic clast	Intermediate	
3.6	364.59	364.63	Volcanic clast	Mafic	Large clinopyroxene
3.6	367.82	367.86	Volcanic clast	Intermediate	Kaersutite
3.6	369.30	369.32	Volcanic clast	Felsic	Large Feldspar
3.6	375.58	375.50	Volcanic clast	Intermediate	
3.6	377.67	377.7	Muddy Diamictite	Clasts with different compositions (mainly intermediate)	Rare Glassy Shards
4.1	402.70	402.75	Volcanic Sandstone	Clasts with different compositions	Sponge Spicules, Glassy brown angular shards, Fragments of crystals
4.1	431.53	431.55	Volcanic Sandstone	Clasts with different compositions	Glassy brown angular shards
4.1	433.19	433.22	Volcanic clast	Felsic	
4.1	434.05	434.08	Volcanic clast	Mafic	Secondary calcite filling of vesicles
4.1	437.16	427.18	Volcanic Sandstone	Clasts with different compositions	Glassy brown shards, calcite cement, Kaersutite rich
4.1	437.46	437.49	Volcanic clast	Mafic	Secondary calcite fills vesicles and replaces olivine
4.1	439.25	439.27	Volcanic clast	Felsic	Kaersutite ghost crystals
4.1	439.29	439.31	Volcanic clast	Mafic	
4.1	439.35	439.38	Volcanic clast	Intermediate	Very fine grained, large kaersutite crystal
4.1	439.51	439.55	Volcanic clast	Mafic	Secondary calcite fills vesicles and replaces olivine
4.1	451.39	451.42	Volcanic clast	Mafic	Secondary calcite fills vesicles and replaces olivine
4.1	454.70	454.76	Volcanic clast	Mafic	Olvine iddingsitised
4.2	461.60	461.63	Volcanic clast		Rounded clast of heterolitic volcanic breccia
4.2	461.84	461.87	Volcanic clast	Felsic	Altered
4.2	465.79	465.83	Volcanic clast	Felsic	Altered, large feldspar phenocrysts
4.2	474.08	474.10	Volcanic clast	Felsic	Altered. Some devitrification texture
4.2	475.26	475.30	Volcanic clast	Intermediate	Secondary calcite replaces Olivine, Kaersutite
4.2	478.52	478.54	Volcanic clast	Mafic	Large altered mafic phenocrysts
4.2	480.09	480.11	Volcanic clast	Felsic	Altered pumiceous clast
4.2	485.28	485.31	Volcanic Mudstone	Clasts with different compositions	Mainly crystal fragments, some glassy shard and pumice
4.2	485.51	485.54	Diamictite	Clasts with different compositions	Mainly crystal fragments, some angular glassy shard
4.2	492.43	492.47	Volcanic Sandstone	Clasts with different compositions	Mainly crystal fragments, some glassy shard and pumice
4.2	497.70	497.73	Volcanic clast	Mafic	Abundant secondary calcite, Large mafic phenocrysts
4.2	504.58	504.62	Diamictite	Clasts with different compositions	Mainly vesiculated brown glassy shard
4.3	511.62	511.65	Volcanic clast	Intermediate	
4.3	518.90	518.91	Volcanic clast	Felsic	Alteration rim and calcite filling of vesicle
4.3	519,00	519.03	Diamictite	Clasts with different compositions	Very heterogenous, felsic and mafic clasts, brown vesiculated shards, crystals (kaersutite, mafic)
4.3	521.48	521.52	Volcanic clast	Intermediate	Secondary calcite fills vesicles and replaces olivine
4.3	527.20	527.22	Volcanic clast	Intermediate	
4.3	527.88	527.92	Diamictite	Clasts with different compositions (mainly felsic)	Abundant pumice clasts
4.3	527.96	528,00	Diamictite	Clasts with different compositions	Pumice and basament clasts
4.3	528.24	528.27	Diamictite	Clasts with different compositions	Very heterogenous
4.3	529.19	529.23	Volcanic Breccia	Clasts with different compositions	Strongly heterolitic, felsic and mafic clasts.
4.3	530.36	530.39	Volcanic clast	Intermediate	Double filling (Cc and Qz) of vesicles
4.3	533.94	533.98	Volcanic Breccia	Clasts with different compositions	Strongly heterolitic, altered felsic and mafic clasts. Glassy rich matrix
4.3	535.75	535.78	Diamictite	Clasts with different compositions (mainly felsic)	Felsic clasts and pumices
4.3	536.17	536.20	Diamictite	Clasts with different compositions	Some altered pumice, crystals
4.3	536.78	536.80	Diamictite	Clasts with different compositions	Some altered pumice, calcite matrix, crystals
4.3	541.97	542,00	Diamictite	Clasts with different compositions	Abundant subrounded brown glassy clasts.
4.3	542.36	542.41	Volcanic clast	Intermediate	Mafic crystals transformed in chlorite
4.4	575.68	575.71	Volcanic Sandstone	Clasts with different compositions	Mainly vesiculated brown glassy shard
4.4	577.14		Volcanic Siltstone	Clasts with different compositions	Almost totally angular brown glassy shards.
4.4	579.25	579.28	Volcanic Sandstone	Clasts with different compositions	Mainly angular glassy shards sometimes tachylitic or pyrite coated. Kaersutite crystals
4.4	584.61	584.64	Volcanic Siltstone	Clasts with different compositions	Almost totally angular brown glassy shards. Calcite cement
5.1	588.34	588.37	Lapilli Tuff	Intermediate	Altered pumiceous clast, Kaersutite, secondary secondary calcite

Tab. 4 - Continued.

LSU	Top	Bottom	Rock Type	Composition on the basis of petrography	Notes
5.1	588.41	588.46	Lapilli Tuff	Intermediate	Altered pumiceous clast, Kaersutite, secondary calcite
5.1	588.63	588.65	Lapilli Tuff	Intermediate	Altered pumiceous clast, Kaersutite, secondary calcite
5.1	589.1	589.15	Lapilli Tuff	Intermediate	Altered pumiceous clast, Kaersutite, secondary calcite, Zeolites
5.1	589.44	589.48	Lapilli Tuff	Intermediate	Secondary calcite
5.1	589.73	589.77	Lapilli Tuff	Intermediate	Altered pumiceous clast, Kaersutite, secondary calcite
5.1	590,00	590.02	Lapilli Tuff	Intermediate	Altered pumiceous clast, Kaersutite, secondary calcite
5.1	590.37	590.4	Lapilli Tuff	Clasts with different compositions (mainly mafic intermediate)	Altered pumiceous clast, Kaersutite, secondary calcite
5.1	591.85	591.87	Lapilli Tuff	Clasts with different compositions (mainly mafic intermediate)	Brown glassy vesiculated granules, crystals, Kaersutite
5.1	592.96	593.01	Volcanic clast	Mafic Nodule	Pyroxenite
5.1	594.18	594.21	Tuffaceous breccia	Clasts with different compositions (mainly mafic intermediate)	Secondary calcite fills vesicles
5.1	595.05	595.09	Tuffaceous breccia	Clasts with different compositions (mainly mafic intermediate)	Secondary calcite fills vesicles
5.1	595.81	595.84	Volcanic Sandstone	Clasts with different compositions (mainly mafic intermediate)	Subrounded palagonitised glassy grains
5.1	599.83	599.86	Volcanic Sandstone	Clasts with different compositions	Angular to subrounded clasts, Lithics, Shells
5.1	600.5	600.53	Lapilli Tuff	Not recognisable	Palagonitised glassy grains, Kaersutite, Silica minerals, Alunite
5.1	601.53	601.56	Lapilli Tuff	Not recognisable	Palagonitised glassy grains, Kaersutite, Silica minerals, Alunite
5.1	602.13	602.16	Lapilli Tuff	Not recognisable	Tube pumices, Palagonitised Glass, Kaersutite, Silica minerals, Alunite
5.1	602.57	602.6	Lapilli Tuff	Not recognisable	Tube pumices, Palagonitised Glass, Kaersutite, Silica minerals, Alunite
5.1	602.79	602.83	Lapilli Tuff	Not recognisable	Tube pumices, Palagonitised Glass, Kaersutite, Silica minerals, Alunite
5.1	602.8	602.83	Lapilli Tuff	Not recognisable	Tube pumices, Palagonitised Glass, Kaersutite, Silica minerals, Alunite
5.1	603.74	603.77	Lapilli Tuff	Not recognisable	Tube pumices, Palagonitised Glass, Kaersutite, Silica minerals, Alunite
5.1	605.39	605.42	Volcanic Sandstone	Clasts with different compositions	Matrix supported, Crystals , Pyrite
5.1	608.73	608.78	Volcanic Siltstone	Clasts with different compositions	Matrix supported, Crystals , Pyrite
5.1	611.35	611.39	Volcanic Sandstone	Clasts with different compositions	Angular to subrounded clasts, Lithics, Pyrite, Crystals from basement
5.1	615.44	615.48	Volcanic Sandstone	Clasts with different compositions	Subrounded clast matrix supported
5.1	618.95	618.98	Diamictite	Clasts with different compositions	Pumiceous clasts altered
5.1	619.72	619.76	Diamictite	Clasts with different compositions	Pumiceous clasts altered
5.1	620.38	620.43	Diamictite	Clasts with different compositions	Pumiceous clasts altered, kaersutite
5.1	620.44	620.49	Volcanic clast	Felsic	Secondary calcite
5.1	621.65	621.68	Tuffaceous breccia	Clasts with different compositions (mainly felsic)	Angular to subrounded clasts matrix supported, Lithics, Pyrite, Crystal from basement, Matrix supported
5.1	622.6	622.63	Volcanic Sandstone	Clasts with different compositions	Angular to subrounded clasts matrix supported, Lithics, Pyrite, Crystal from basement, Matrix supported
5.1	622.93	622.95	Volcanic Sandstone	Clasts with different compositions	
5.1	623.47	623.49	Siltstone		Crystal rich lamination, green glauconite
5.1	624.02	624.05	Volcanic Sandstone		
5.1	636.4	636.42	Volcanic Sandstone	Clasts with different compositions	Altered pumiceous clast, Kaersutite, Calcite
5.1	636.77	636.79	Mudstone		Few volcanics
5.1	641.44	641.48	Tuffaceous breccia	Clasts with different compositions	Subangular -subrounded palagonitised pumiceous clasts
5.1	642.39	642.42	Volcanic clasts in mudstone	Felsic	Clasts resembling underlying lava flow
5.1	644.14	644.15	Crystal-rich mudstone		
5.1	645.74	645.77	Volcanic clasts in mudstone	Felsic	Clasts resembling underlying lava flow
5.1	646.24	646.28	Volcanic clasts in mudstone	Felsic	
5.2	646.38	646.41	Lava rim	Felsic	
5.2	646.38	646.41	Lava rim	Felsic	Lava flow glassy rim
5.2	647.56	647.58	Lava	Felsic	Flow banding
5.2	649.29	649.32	Lava	Felsic	Lava flow glassy rim
5.3	652.81	652.83	Volcanic Sandstone	Clasts with different compositions (mainly felsic)	Matrix supported
5.3	656.66	656.58	Volcanic Breccia	Clasts with different compositions (mainly felsic)	Palagonitised glassy vesicled clasts, Matrix supported
5.3	656.99	657.02	Volcanic Siltstone	Clasts with different compositions (mainly felsic)	Palagonitised glassy vesicled clasts, Matrix supported
5.3	657.56	657.59	Volcanic Sandstone	Clasts with different compositions (mainly felsic)	Palagonitised glassy vesicled clasts, Matrix supported
5.3	658.02	658.04	Volcanic Sandstone	Clasts with different compositions (mainly felsic)	Red Clasts
5.3	660.86	660.9	Volcanic Sandstone	Clasts with different compositions (mainly felsic)	Abundant crystals, Red Clasts
5.3	662.65	662.69	Volcanic Sandstone		Abundant crystals, Palagonitised glass
5.3	663.03	663.03	Volcanic Sandstone		Abundant crystals, Palagonitised glass
5.3	663.23	663.26	Volcanic Sandstone		Abundant crystals, Palagonitised glass
5.3	663.91		Volcanic Breccia	Clasts with different compositions (mainly intermediate)	Large mafic crystals, Palagonitised glassy pumiceous clasts
5.3	668.01	668.05	Volcanic Sandstone		Abundant crystals, Palagonitised glass
5.3	678.35	678.38	Diamictite	Clasts with different compositions (mainly intermediate-felsic)	Subangular-subrounded palagonitised pumiceous clasts and light pumices

Tab. 4 - Continued.

LSU	Top	Bottom	Rock Type	Composition on the basis of petrography	Notes
5.3	678.90	678.93	Diamictite	Clasts with different compositions (mainly felsic)	Subrounded ligth pumices
5.3	679.68	679.71	Diamictite	Clasts with different compositions (mainly felsic)	Pumices and subangular clasts of aphyric glassy lava
5.3	680.36	680.40	Diamictite	Clasts with different compositions (mainly felsic)	Pumices and clasts of aphyric glassy lava
5.3	681,00	681.03	Diamictite	Clasts with different compositions (mainly felsic)	Pumices and clasts of aphyric glassy lava. Large mafic crystal
5.3	681.40	681.44	Diamictite	Clasts with different compositions (mainly felsic)	Pumices and clasts of aphyric glassy lava. Large mafic crystal
5.3	681.57	681.61	Volcanic clast	Felsic	Fine grained
5.3	681.63	681.67	Diamictite	Clasts with different compositions (mainly intermediate-felsic)	Abundant Pumices, Clast of coarse tuff
5.3	683.38	683.41	Volcanic Siltstone		Almost all palagonitises glassy subrounded shards
5.3	688.80	688.83	Volcanic Siltstone		Almost all palagonitises glassy subrounded shards, Pumices, Crystals
5.4	692.74	692.78	Volcanic Siltstone		Almost all altered glassy subrounded shards, Crystals
5.4	696.92	696.96	Volcanic Siltstone	Felsic	Almost all altered glassy subangular shards, crystals and pumices
5.4	702.19	702.22	Volcanic Siltstone		Almost all altered glassy subrounded shards, crystals, kaersutite and pumices
5.4	715.05	715.08	Volcanic Siltstone	Felsic	Pumices matrix-supported
5.4	716.23	716.27	Volcanic Siltstone		Angular glassy shards
5.4	720,00	720.04	Volcanic Siltstone		Angular glassy shards
5.4	725.07	725.08	Volcanic clasts in mudstone	Clasts with different compositions (mainly intermediate-felsic)	
5.4	728.01	728.04	Volcanic clasts in mudstone	Mafic	
5.4	744.06	744.1	Volcanic Sandstone	Clasts with different compositions (mainly intermediate-felsic)	Pumicoeus clasts
5.4	745.12	745.16	Volcanic Sandstone	Clasts with different compositions	Some pumices
5.4	747.09	747.13	Volcanic Sandstone	Clasts with different compositions	Some pumices
5.4	748.97	749,00	Volcanic Sandstone	Clasts with different compositions (mainly intermediate)	
5.4	758.08	758.11	Volcanic Sandstone	Mostly felsic clasts	
6.1	773,00	773.06	Volcanic clast	Mafic	
6.1	775.49	775.51	Volcanic clast	Intermediate	Kaersutite
6.1	778.70	778.73	Mudstone		
6.1	778.80	778.82	Volcanic clast	Felsic	
6.1	782.77	782.79	Volcanic clast	Intermediate	
6.1	792.48	792.51	Diamictite		Volcanic and non volcanic clasts, some pumices altered
6.1	796.63	796.65	Volcanic clast	Felsic	Secondary calcite fills vesicles
6.1	804.07	804.10	Volcanic Mudstone	Clasts with different compositions (mainly felsic)	Crystal rich, mainly mafic
6.1	819.48	819.51	Volcanic Sandstone	Clasts with different compositions	
6.1	820.06	820.09	Diamictite	Clasts with different compositions (mainly intermediate-felsic)	Crystal rich
6.1	821.50	821.52	Diamictite	Clasts with different compositions	Crystal rich
6.1	822.24	822.26	Diamictite	Clasts with different compositions	2 clasts
6.1	825.52	825.54	Muddy Diamictite	Felsic-mafic	Few Clasts
6.1	826.77	826.79	Volcanic clasts in mudstone	Felsic	Altered sharp shapes of clasts
6.1	826.97	827,00	Volcanic clast	Mafic	
6.1	831.59	831.62	Volcanic clast	Mafic	
6.1	837.17	837.2	Volcanic clast	Intermediate	Kaersutite
6.1	850.38	850.41	Volcanic Sandstone		Crystal rich, mainly mafic
6.1	853.69	853.71	Volcanic clast	Felsic	
6.1	856.36	856.38	Volcanic clast	Felsic	Calcite and Pyrite
6.1	861.7	861.71	Volcanic clast	Felsic	
6.1	875.72	875.74	Volcanic clast	Clasts with different compositions (mainly felsic)	Acmite and Tube Pumices
6.1	883.74	883.75	Volcanic clast	Felsic	Acmite
6.1	887.17	887.19	Volcanic clast	Intermediate	Calcite
6.2	899.03	899.05	Volcanic clast	Felsic	Calcite
6.2	905.01	905.02	Diamictite clast		Pumices
6.2	913.07	913.08	Diamictite clast		Pumices
6.3	922.19	922.20	Volcanic clast	Intermediate	
6.3	932.17	932.21	Volcanic clast	Felsic	Secondary calcite fills vesicles
6.3	932.47	932.52	Volcanic clast	Intermediate	Secondary calcite fills vesicles
6.3	943.24	943.27	Volcanic clast	Intermediate	Pumiceous clasts
6.3	944.36	944.38	Diamictite		Mainly crystals, rare pumice
6.3	949.47	949,00	Diamictite clast		
6.3	971.92	971.93	Volcanic clast	Felsic	Secondary calcite fills vesicles
6.3	979.72	979.74	Volcanic clast	Felsic	Pyrite
6.3	981.34	981.35	Volcanic clast	Felsic	Secondary calcite fills vesicles
6.3	1003.11	1003.14	Volcanic clast	Intermediate	Secondary calcite replaces olivine
6.3	1004.08	1004.09	Volcanic clast	Felsic	Devetrification texture
6.3	1047.48	1045.51	Diamictite	Clasts with different compositions	Most clasts are altered
6.3	1062.63	1062.66	Diamictite	Clasts with different compositions (mainly felsic)	Most clasts are altered
6.4	1065.31	1065.32	Volcanic Clast	Felsic	
6.4	1065.78	1065.8	Volcanic Clast	Felsic	
6.4	1077.35	1077.36	Diamictite	Clasts with different compositions (mainly intermediate-felsic)	Several non volcanic clasts

Tab. 4 - Continued.

LSU	Top	Bottom	Rock Type	Composition on the basis of petrography	Notes
6.4	1079.74	1079.76	Volcanic Clast	Intermediate	Secondary calcite filling of vesicles, large mafic phenocrysts
6.4	1080.57	1080.59	Diamictite	Clasts with different compositions	Some pumice several non volcanic clasts
6.4	1087.02	1087.07	Volcanic Clast	Mafic	Large mafic crystals
6.4	1087.25	1087.28	Volcanic Clast	Felsic	
6.4	1106.66	1106.69	Volcanic Clast	Mafic	Secondary calcite filling of vesicles, large mafic phenocrysts
6.4	1113.18	1113.21	Volcanic Clast	Felsic	Secondary calcite filling of vesicles
6.4	1114.68	1114.71	Volcanic Clast	Felsic	Acmite
6.4	1115.27	1115.29	Volcanic Clast	Intermediate	Large mafic crystals
6.4	1121.40	1121.43	Diamictite	Clasts with different compositions (mainly felsic)	
6.4	1122.09	1122.12	Volcanic Clast	Felsic	Large sanidine, Arfersonite
6.4	1123.59	1123.61	Volcanic Clast	Felsic	Acmite
6.4	1131.40	1131.42	Volcanic Clast	Felsic	Large sanidine, Arfersonite (MCI)
6.4	1137.05	1137.08	Volcanic Clast	Felsic	
6.4	1139.63	1139.65	Volcanic Clast	Felsic	
6.4	1139.88	1139.91	Volcanic Clast	Felsic	Altered
6.4	1149.88	1149.91	Diamictite	Clasts with different compositions (mainly intermediate)	
6.4	1163.67	1163.69	Volcanic Clast	Felsic	
6.4	1164.33	1164.36	Subvolcanic	Felsic	
6.4	1166.50	1166.52	Diamictite	Clasts with different compositions (mainly felsic)	Large clast with sanidine
6.4	1180.58	1180.61	Volcanic clast	Intermediate	Large plagioclase
6.4	1192.55	1192.57	Volcanic clast	Felsic	Secondary calcite filling of veins and vesicles
6.4	1200.11	1200.13	Clast of breccia		Almost totally made of volcanic clasts
6.4	1203.58	1203.60	Volcanic clast	Felsic	
6.4	1212.64	1212.67	Volcanic Clast	Intermediate	Altered
6.4	1216.59	1216.60	Volcanic clast	Intermediate	Large feldspars
6.4	1219.87	1219.88	Volcanic clast	Felsic	Large strongly corroded feldspars
7.1	1221.20	1221.22	Volcanic sandstone		Strongly heterolithic, with abundant basament clasts and minerals. Silica minerals and calcite patches
7.1	1221.53	1221.56	Volcanic clast	Clasts with different compositions (mainly intermediate)	Most clasts are subangular altered pumices. Some are fragments of a palagonitised glassy tuff. Silica mineral form cement.
7.1	1221.87	1221.89	Volcanic sandstone		Strongly heterolithic, with abundant basament clasts and minerals. Silica and calcite patches
7.1	1221.96	1222,00	Volcanic sandstone		Strongly heterolithic, with abundant basament clasts and minerals.
7.1	1222.14	1222.17	Lapilli Tuff	Intermediate	Mostly subangolar palagonitised clasts, secondary silica minerals
7.1	1222.68	1222.70	Lapilli Tuff	Clasts with different compositions (mainly intermediate)	Abundant crystals and clasts from basement. Calcite patches
7.1	1222.76	1222.81	Lapilli Tuff	Intermediate	Sunrounded palgonitised lapilli in palagonitised ash matrix. Silica minerals and calcite fill veins or form cements
7.1	1222.95	1222.98	Lapilli Tuff	Intermediate	Subangolar palagonitised clasts, Silica cement
7.1	1222.98	1223.00	Volcanic sandstone		Strongly heterolithic, with abundant basament clasts and minerals. Silica and calcite patches
7.1	1227.26	1227.28	Tuff		Subangular, sometimes fluidal, poorly vesiculated glass shard
7.1	1236.16	1236.21	Tuff	Intermediate	Clasts are subangular and palagonitised. Calcite form cement
7.1	1237.51	1237.55	Lapilli Tuff	Intermediate	Strongly palagonitised, Silica cement
7.1	1238.01	1238.04	Tuff	Felsic	Angular and subangular palagonitised glassy shardså, abundant free crystals, Silica cement
7.1	1240.66	1240.69	Tuff	Felsic	Angular glassy shards, abundant free crystals, Silica cement
7.1	1242.78	1242.82	Lapilli Tuff	Felsic	Angular palagonitised and vesicular glassy clasts, silica and calcite patches
7.1	1246.63	1246.66	Tuff	Felsic	Angular and subangular glassy shards sometimes palagonitised, abundant free crystals, Silica cement
7.1	1248,00	1248.05	Lapilli Tuff	Felsic	Subangolar glassy clasts, Silica cement
7.1	1249.06	1249.09	Lapilli Tuff	Felsic	Subangolar glassy clasts, Silica cement
7.1	1254.75	1254.78	Tuff	Felsic	Angular and subangular palagonitised glassy shards, abundant free crystals, Silica cement
7.1	1255.21	1255.24	Tuff	Felsic	Angular and subangular palagonitised glassy shards. Pyrite rich
7.1	1258.8	1258.84	Tuff	Felsic	Angular and subangular palagonitised glassy shards, abundant free crystals, Silica cement
7.1	1262.28	1262.32	Tuff		Angular and fluidal shape palagonitised glassy shards
7.1	1263.96	1263.96	Tuff		Angular palagonitised brown and ligth glassy shards, calcite patches
7.1	1264.90	1264.93	Tuff		Angular palagonitised brown and ligth glassy shards, calcite patches
7.1	1266.71	1266.75	Tuff		Subangolar palagonitised glassy clasts, Silica cement
7.1	1269.71	1269.76	Tuff		Subangolar palagonitised glassy clasts, Silica cement
7.1	1272.11	1272.14	Tuff		Subangolar palagonitised glassy clasts, Silica cement
7.1	1274.38	1274.39	Volcanic Clast	Felsic	
8.1	1277.91	1277.95	Volcanic Clast	Felsic	Large sanidine, acmite
8.1	1278.04	1278.06	Volcanic Clast	Felsic	
8.1	1278.84	1278.87	Volcanic Clast	Felsic	
8.1	1279,00	1279.04	Volcanic Clast	Felsic	Large sanidine, acmite
8.1	1284.71	1284.72	Volcanic Clast		

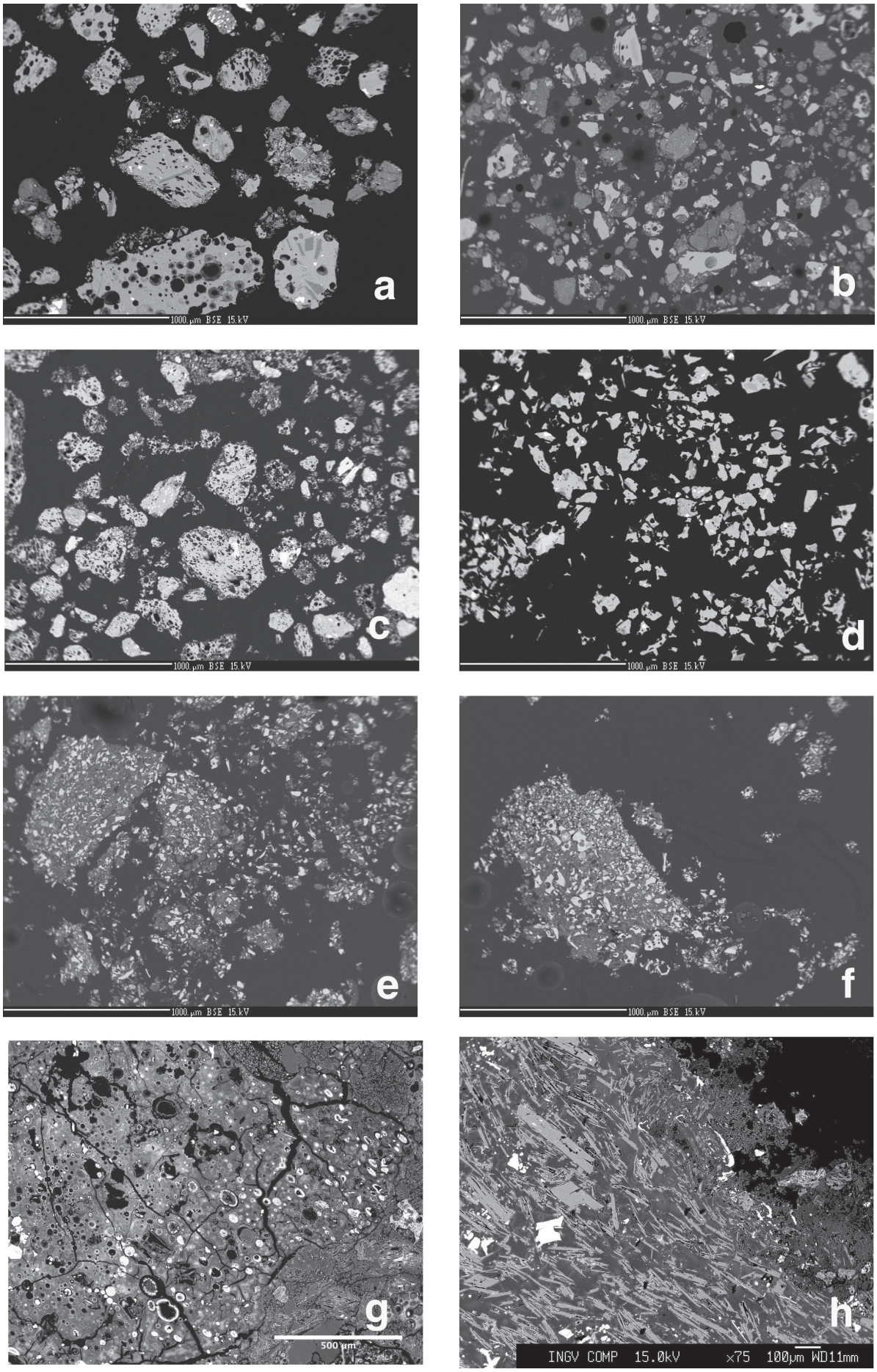

Fig. 7 – Backscatter images of grain mounts (a-f) and thin sections (g-h) from selected volcanic layers.: (a) 25.56 mbsf; (b) 56.50 mbsf; (c) 85.80 mbsf; (d) 114.47 mbsf; (e) 431.51 mbsf; (f) 577.14 mbsf; (g) altered volcanic clast at 602.80 mbsf; (h) glassy rim in lava flow at 646.38 mbsf.

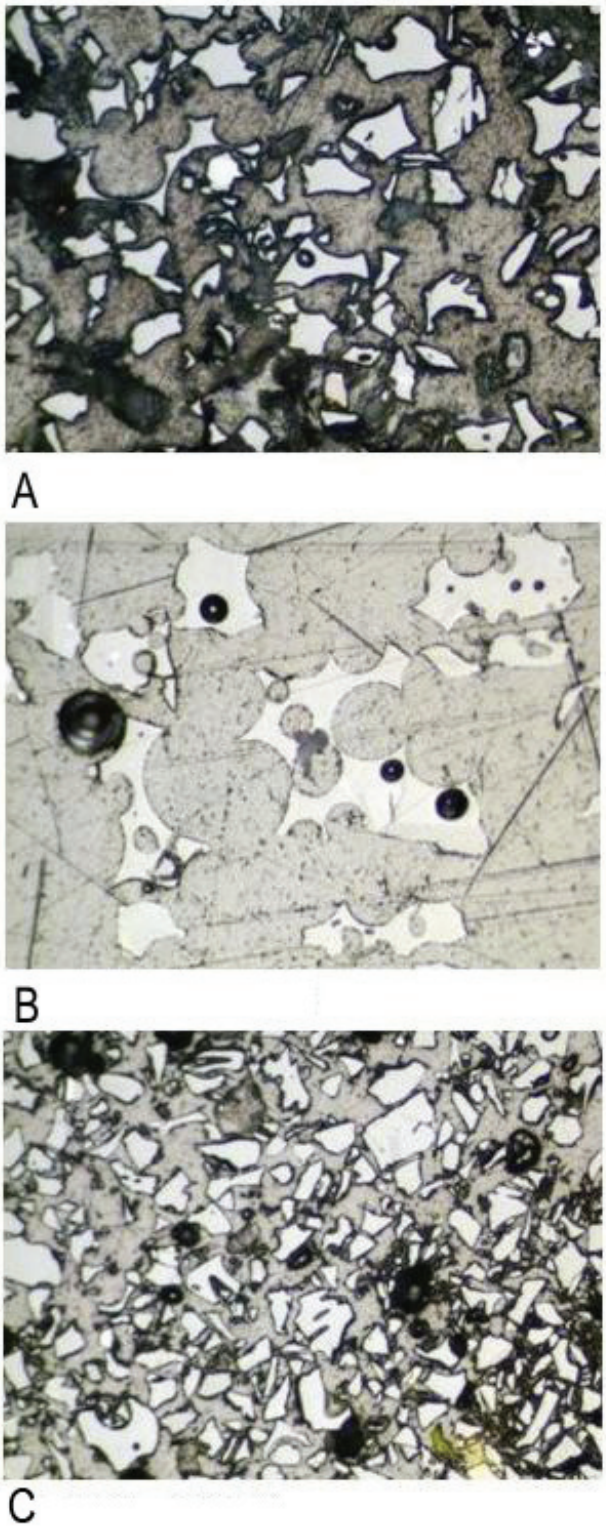

Fig. 8 – Polished grain mounts of glass shards between 140 and 146 mbsf in AND-1B core. A) 140.30 m (100x); B) 145.12 m (100x); C) 142.77 (100x).

Lithostratigraphic Subunit 2.4 (132.83-146.79 mbsf)

This interval is almost totally (>95%) made of volcanic detritus (sandstones, siltstones, and mudstones). Grains in these beds are angular glassy shards sometimes showing fluidal delicate shapes (Fig. 8). Larger sand grains are very vesicular. Glass is pale brown, and, as it contains local microphenocrysts of clinopyroxene, plagioclase, and minor kaersutite, it can be classified as basanite-tephrite on the TAS diagram (Fig. 6).

Lithostratigraphical Subunit 3.1 (146.79-169.4 mbsf)

Mafic clasts and mafic glassy granules are present in shallow layers (<149 mbsf) of this LSU. Glassy rims on mafic clasts suggest subaqueous emplacement. At depths greater than 149 mbsf intermediate and felsic volcanic clasts dominate. Felsic and intermediate rocks show trachytic textures and sometime large (>2 mm) feldspar phenocrysts. Secondary calcite, silica minerals, and pyrite fill vesicles and/or veins.

Lithostratigraphical Subunit 3.2 (169.4-181.93 mbsf)

In this interval, volcanic clasts, mainly lonestones, occur in diatomite. They show a large variability in composition ranging from mafic (more abundant) to felsic lithologies. Brown glass shards are recognisable in volcanic mudstone.

Lithostratigraphical Subunit 3.3 (181.93-292.66 mbsf)

This subunit contains a short interval (184.6–184.9 mbsf) of bedded and normally graded glassy volcanic sandstone and siltstone, as well as abundant volcanic clasts dispersed in sediment. Glassy shards (at 184.7 mbsf) show a basanite/tephritic composition. Volcanic clasts in this subunit show a bimodal composition with both mafic and felsic rocks. Mafic clasts contain large (>1 mm) pyroxene and olivine phenocrysts. Olivine is commonly replaced by carbonates. Felsic fragments show trachytic textures and occasionally large feldspar phenocrysts. Altered pumice clasts are also found in diamictite in the upper part of the subunit (188–189 mbsf). Subangular and subrounded brown glassy shards occur in variable abundance in diamictite or in sandy mudstone**.** On the whole, felsic rock clasts fragments dominate at depths less than 200 mbsf, while mafic compositions are dominant downward.

Lithostratigraphical Subunit 3.4 (292.66-347.19 mbsf)

Volcanic pebbles in diamictite are generally fresh and bimodal in composition with approximately the same number of mafic and felsic clasts, between those sampled. Clasts with red oxidised groundmass are also present. Clasts smaller than granule show an intermediate-felsic composition and are frequently pumiceous and glassy. In the diamictite matrix, free crystals are also abundant. Secondary calcite replaces some olivine and fills vesicles, and veins.

Lithostratigraphical Subunit 3.5 (347.19-363.37 mbsf)

Volcanic granules in diamictite are very heterogeneous, and include brown vesiculated glass, felsic fine-grained rocks, tube pumice, and red oxidised clasts. Free crystals, including acmite and kaersutite, are also abundant.

Lithostratigraphical Subunit 3.6 (363.37-382.98 mbsf)

Volcanic granules in diamictite are mainly intermediate in compositions and glassy shards are rare. Volcanic pebbles are mainly intermediate in composition. Mafic clasts have large millimetre-size crystals of clinopyroxene.

Lithostratigraphical Subunit 4.1 (382.98-459.24 mbsf)

Silt-bearing diatomite in the middle of this interval contains fresh, angular glassy shards with basanitic composition (Fig. 6 & Fig. 7e). In the lower part of the succession, *c.* 437 mbsf calcite-cemented volcanic sand is composed of fresh brown, subrounded vesicular shards. Kaersutite fragments are abundant in this horizon. Granules and pebbles in diamictite are mainly mafic in composition. Secondary calcite commonly fills vesicles and replaces large (>2 mm) olivine crystals.

Lithostratigraphical Subunit 4.2 (459.24-511.18 mbsf)

Volcanic pebbles in diamictite-diatomite include felsic clasts characterised by large (>1 mm) feldspar phenocrysts set in a trachytic texture with devitrified glass and mafic clasts with large olivine and pyroxene phenocrysts. A rounded clast made of heterolithic volcanic breccia is present. Volcanic sand (*c.* 482–504 mbsf) is composed of crystal fragments, fresh brown glass shards, and rare pumices. Shards are vesiculated and subangular and have a trachytic composition (Fig. 6).

Lithostratigraphical Subunit 4.3 (511.18-575.11 mbsf)

Volcanic pebbles in diatomite-diamictite are mainly intermediate in composition, with secondary calcite and silica typically filling vesicles. Granule and smaller clasts in diamictite are largely heterolithic and contain mafic and felsic fragments, as well as deeply altered pumices and occasionally basement clasts. Coarse sandy layers contain vesiculated brown glass. Calcite is abundant in matrix or as alteration product in olivine.

Lithostratigraphical Subunit 4.4 (575.11-586.45mbsf)

In this interval, volcanics are present only as siltstones and sandstones. They are mainly composed of fresh brown angular glassy shards with basanitic composition (Fig. 6 & 7f). Secondary calcite patches are also widespread.

Lithostratigraphical Subunit 5.1 (586.45-646.49 mbsf)

Volcanic detritus in this subunit is mainly concentrated in two distinct intervals with a homogeneous composition and angular or subangular shape. These features are interpreted to represent syn-eruptive resedimentation after limited transport of a primary autoclastic deposit. The deposit at interval 588–593 mbsf is made of altered intermediate pumiceous clasts. These clasts contain phenocrysts of plagioclase, pyroxene, and kaersutite set in a glassy groundmass, totally replaced by calcite. Fragments of kaersutite are also common within this deposit. Lower beds below (*c.* 590–593 mbsf) pumiceous clasts change in composition (Fig. 6). Mafic phenocrysts are more abundant, and glass (brown) appears fresh. Lapilli tuff between 600 and 603 mbsf is made of totally palagonised glassy clasts, which hampered even a rough estimate of the composition (Fig. 7h). However, the occurrence of kaersutite crystal fragments and the presence of tube pumices suggest a felsic composition. This subunit also comprises numerous volcanic sandstones and mudstones. These deposits are made of angular to subrounded glassy grains, heterogeneous finely crystallised lithics, crystal fragments, and negligible basement clasts. Mudstones at the bottom of the subunit contain felsic scoriaceous clasts showing mineral assemblages and textures comparable with those of the underlying lava flow. Throughout this subunit, calcite, silica minerals, and locally K-Al sulfate (alunite) fills vesicles of volcanic rocks or form cement between clasts (Fig. 7g). Pyrite is abundant.

Lithostratigraphic Subunit 5.2 (646.49-649.3 mbsf)

The lava flow is a fine-grained intermediate rock with few large (>1 mm) feldspar phenocrysts set in a trachytic groundmass. Upper and lower contacts show a glassy rim, now replaced by clay minerals (Fig. 7h). Secondary calcite and silica minerals fill vesicles and veins. The occurrence of glassy rims, flow and shear textures and some reworking of the upper scoriaceous portion allowed us to classify this volcanic bed as a submarine lava flow.

Lithostratigraphic Subunit 5.3 (649.3-688.92 mbsf)

Volcanic rocks in this interval form clasts in sandstone, siltstones, and diamictite. In the upper part (<669 mbsf) where siltstone and sandstone are more abundant, clasts are mainly subangular to subrounded palagonised light brown glass with subordinate light pumice and finely crystallised lithics, locally red. Free crystals are also copious, and calcite and alunite fill vesicles and veins. Diamictites and related fine-grained deposits in the lower part of the interval contain light rounded pumice and aphyric fine-grained felsic clasts. These latter clasts are not vesiculated and show curviplanar edges. All these characteristics can be related to the reworking and resedimentation of autoclastic material related to the emplacement of a submarine lava flow or to a volcanic dome.

Lithostratigraphic Subunit 5.4 (688.92-759.32 mbsf)

In this subunit volcanics occur in siltstones and sandstones as angular to subrounded grains. Clasts include light glassy pumices, brown poorly

vesiculated glass shards, or finely crystallised black or red lithics. Fragments of crystals (feldspars or green pyroxenes) are also present. Lonestones in mudstone deposits range from mafic to felsic.

Lithostratigraphic Subunit 6.1 (759.32-897.95mbsf)

This interval is characterised by a low content of volcanic detritus and, at least in the upper layers (<850 mbsf) by a large compositional variability. Pebbles range from intermediate to felsic with rare mafic clasts. Felsic rocks are medium grained and show well-developed trachytic texture. Secondary calcite fills vesicles and veins. Sand grains and granules in diamictites show a large compositional variability. Basement clasts and minerals are important components and intermediate and felsic clasts are the also well represented. In some mudstones (*e.g.* 826.77 mbsf) very angular altered pumice occurs. Below 850 mbsf felsic pebbles are the most abundant. They are fine grained and have a well-developed trachytic texture with acmite microphenocrysts between flow-aligned feldspar laths. Calcite patches and pyrite are also dispersed.

Lithostratigraphical Subunit 6.2 (897.95-920.51 mbsf)

McMurdo volcanic rocks in this interval are limited to some felsic pebbles. These clasts are altered and show calcite filling of vesicles. Resedimented diamictite clasts contain deeply altered pumice fragments and both mafic and feldspar free crystals.

Lithostratigraphical Subunit 6.3 (920.51-1063.42mbsf)

In this subunit volcanics occur as pebbles and granules in diamictite. They have a composition ranging from intermediate to felsic. These rocks are fine grained with few feldspar and mafic phenocrysts (*c.* 1 mm). Secondary calcite filling vesicles is abundant. Sand grains in diamictite are very variable and include altered pumice, McMurdo volcanics, basement clasts and subrounded mineral fragments.

Lithostratigraphical Subunit 6.4 (1063.42-1220.15 mbsf)

Volcanic rocks in this interval occur mainly as clasts in the diamictite. Pebble-size clasts show a predominant felsic composition. These clasts have large (>1 mm) feldspar phenocrysts set in a trachytic groundmass. Acmite or arfedsonite crystals are sometimes present. Mafic and intermediate rocks are characterised by large (>1 mm) mafic phenocrysts. Calcite filling of vesicles and veins are ubiquitous.

Lithostratigraphical Subunit 7.1 (1220.15-1275.24 mbsf)

Volcanic rocks in subunit 7.1 comprise tuffs, lapilli tuff and minor sandstone. Clasts in tuffs and lapilli tuffs are generally homogeneous in composition. They are palagonised angular to subangular grains, with a large range of vesicularity. In upper part of the interval (<1238 mbsf) clasts are made mostly of brown glass with some microphenocrysts of feldspars and mafic phases. We classify these clasts as intermediate in composition. Below 1 238 mbsf composition appears more felsic, as brown glass contains only feldspar and some light-coloured glassy grains are present. Between clasts and within vesicles, secondary calcite, silica minerals, and pyrite are abundant. Sandstones, mainly concentrated at a depth of 1 222 mbsf, are strongly heterolithic with volcanic clasts, basements grains, and crystals.

Lithostratigraphical Subunit 8.1 (1275.24-1284.87 mbsf)

In this interval only few volcanic clasts in diamictite were found. They are felsic in composition and consist of medium-grained porphyritic rock with large feldspars (>2 mm) and subordinate acmite phenocrysts set in a trachytic groundmass.

SUMMARY

1. A significant amount of McMurdo Volcanic Group detritus occurs in the core. For example, volcanic glass is common in smear slides from a large number of stratigraphic units and volcanic clasts dominate (over 70% in abundance; see Tab. 2). This is consistent, as numerous volcanic centres on Ross Island, White Island, and vents to the south, especially Minna Bluff, surround the drill site. Most of the volcanic detritus is related to the erosion, transport, and deposition by glacimarine sedimentary processes.
2. Compositionally, the volcanic clasts are not diagnostic of any particular eruptive centre, but Ar/Ar dating should help identify the centres and thus provide insight into ice transport paths for constituents of diamictites.
3. There is not an extensive record of primary pyroclastic fallout deposits (volcanic ashes/tephra) that is consistent with the non-explosive nature of the McMurdo Volcanic Group vents in the area. One important exception is discussed below (point 6). No eruptive materials from Erebus volcano were found.
4. A basaltic hyaloclastite clast and associated glass from 25 mbsf is believed to come from a nearby submarine vent. We suggest the vent is a small, currently buried feature imaged on a seismic profile *c.* 3 km to the south of the drill site (Henrys, personal communication).
5. A felsic pumice layer at 85 mbsf and dated at 1.015 Ma (Wilson et al. 'Preliminary Integrated Chronostratigraphy', this volume) cannot be correlated to any known vent onshore but is likely to be derived from somewhere on Ross Island, as no 1 Ma felsic eruptive vents are known south of the drill site. The only exposed felsic rock at the nearby Hut Point Peninsula is Observation Hill that has an age of 1.2 Ma. Phonolite vents are widespread on Mount Terror and are a likely source

area although there could be *c.* 1 Ma vents on Hut Point Peninsula and elsewhere on Ross Island that are now covered by ice and snow.

6. The black well-sorted volcanic sands of lithostratigraphical subunit 2.4 from (132.83 to 146.79 mbsf) were in the main derived from subaerial Hawaiian/Strombolian-type eruptions. The graded bedding in the units, although interpreted in the stratigraphic discussion as due to mass flow such as turbidity currents, may represent fallout of tephra through a water column. Sorting during settling through a water column would account for the normally graded beds. The delicate nature of the glass shards (Fig. 8) in four representative samples is inconsistent with any mass flow process, as this would destroy the classic shard forms. We interpret lithostratigraphical subunit 2.4 as representing a very rapid accumulation perhaps from a nearby vent. The source of these *c.* 2 Ma tephra is unknown.
7. The occurrence of the lava flow places constraints on the maximum distance from the eruptive vent (*c.* 4 km at maximum, according to average length of the lava flow with similar composition; Walker, 1973).
8. Alteration and diagenetic processes modified significantly textures and compositions of the lower section (>600 mbsf) of the core. This limits our understanding of magma evolution and provenance, and makes both radiometric and magnetic age determination difficult.

CONTINUOUS GEOCHEMICAL MEASUREMENT WITH XRF CORE SCANNER AND COLOUR REFLECTANCE DATA

To infer palaeoclimatic information from chemical characteristics of sediment cores it is necessary to obtain the most continuous and accurate measurements (Roehl & Abrams 2000). High-resolution studies provide important datasets for recognising rapid palaeoclimatic changes in the Antarctic environment. Chemical elements are good indicators of such changes. The different sedimentary conditions could be improved by using, for example, Si as an indicator for biogenic primary production. Zr and Sr typically indicate volcanic material like ashes from surrounding volcanoes, whereas other elements, such as Fe, Ca, and K, represent the presence of terrigenous ice-transported or diagenetic material. To get this information out of the ANDRILL AND-1B core we used a nondestructive, mobile, AVAATECH XRF core scanner on the ice. The core scanner detects the chemical composition on the surface of split cores. The scanner is able to measure chemical elements between Al (atomic no. 13) and U (atomic no. 92) (http://www.avaatech.com) with reliable values between Al and Ba (atomic no. 56) (Richter in press). Between 27 October and 28 December 2006, continuous measurements were carried out on the archive halves of the AND-1B drill core shortly after splitting with resolutions between 0.5 and 10 centimetres (cm). In the following paragraphs, measurement settings and methods will be discussed.

Below, we present data for the methodical quality assurance, which is important to produce reliable data sets.

METHODS

Instrument Settings

The AAVATECH XRF core scanner generates X-rays with a forced, air-cooled Oxford 50 Watt X-ray source with a rhodium anode and a voltage and current range of 4 to 50 kV and 0 to 1 mA, respectively. Different excitations were used to achieve optimum energy levels for individual element ranges without exceeding a dead-time above 40% (Tab. 5). Dead-time is the percentage of counts not used for processing due to limited speed of the electronics. Filters could be placed in the beam path before targeting the sample surface. Between X-ray source, sample surface, and detector, a helium-flushed prism was mounted to form a pseudo vacuum transmission medium for the X-ray and X-ray fluorescence. The X-ray fluorescence was measured with an energy dispersive (EDX) Amptek XR-100CR X-ray detector (5 mm^2, 0.5 mil Be window/500 µm/2-stage Peltier cooler, internal Ag collimator, 1.5 inch detector extension), a PX2CR power supply and an amplifier with 20 µs shaping time and a MCA8000A multichannel analyser.

Measuring intervals varied between 0.5 and 10 cm depending on occurring lithologies and core conditions. Measuring spot size (= irradiated area) was usually 1 × 1 cm but set to 0.5 × 1 cm when measuring intervals were below 1 cm (*i.e.* between 196.49 and 198.43 mbsf). This is large enough to minimise the effect of mineral heterogeneities (Ge et al. 2005). Measurements were carried out at 10 and 50 kV, and occasionally at 30 kV to analyse additional elements (see Tab. 6). To achieve high-resolution spectra a copper filter was placed in the X-ray beam that was set at 50 kV. For the occasional 30 kV measurements a thick Pd filter was used, but for the 10 kV energy setting, no filter was used. Measuring times were 30 s for both the 10 and 30 kV energy levels and 40 s for the 50 kV level. Energy spectra were saved individually for each of the *c.* 21 000 measurement points.

Tab. 5 - XRF measurement settings.

Setting no.	*X-ray excitation*	*X-ray excitation*	*Filter*	*Count time*	*Elements*
	kV	mA		sec	from - to
A	10	0.3	-	30	Al – Rh
B	50	0.7	Cu	30	Sr – Ba
C	30	1	Pd-thick	40	Fe – Bi

Tab. 6 - Elements detected and statistics.

Element	Min. [counts]	Max. [counts]	Total Number	Mean [counts]	Std. Deviation	Setting [s.Tab.5]
Al	47	1337	15204	353	90	A
Si	42	11344	15204	1273	826	A
S	1	2073	12061	144	129	A
Cl	227	27742	20475	7959	3047	A
Ar	3	3575	20467	256	122	A
K	17	22698	15204	3085	1874	A
Ca	691	87190	15204	8329	6123	A
Ti	25	13571	20475	3670	1986	A
Cr	8	674	20472	145	56	A
Mn	1	4489	20404	577	313	A
Fe	146	63573	20471	27248	8318	A
Co	1	1006	20458	356	103	A
Rh	817	5896	20471	2690	442	A
Sr	6	25670	20451	423	457	B
Zr	2	4274	20464	381	188	B
Ag	1032	4576	20418	3290	379	B
Sn	241	1773	20371	869	96	B
Te	28	332	20473	142	34	B
Ba	21	18866	20390	839	391	B
Fe	188	24619	968	10464	2915	C
Ni	37	137	968	78	15	C
Cu	1	69	968	15	8	C
Zn	2	148	968	60	17	C
Br	4	99	968	29	11	C
Rb	2	888	967	335	166	C
Sr	151	7428	968	1442	561	C
Zr	212	10316	968	1969	853	C
Ru	1160	3090	968	1894	237	C
Rh	872	1944	968	1464	116	C
Pb	6	166	968	23	10	C

Sample Preparation

The nondestructive XRF core-scanning measurements were obtained directly at the split core surface of the archive half covered by a 4 µm SPEXCerti Prep Ultralene® film after the core surface was cleaned. This film avoids contamination of the prism that moves to the sample points downcore. The sediment surface below the film was smoothened if possible and air bubbles and water were squeezed out.

Data Processing and Element Detection

A data file was created at every measurement containing the collected counts per spectral channel and the instrument setting information. These spectra were processed to obtain X-ray intensity data for individual elements. This is done with the WinAxil and WinAxilBatch (CANBERRA NV/SA, Belgium) software and consists of subtracting a background curve, applying statistical corrections for physical processes in the detector, deconvolution of overlapping peaks, calculation of peak integrals, and storage of the results. For each measurement setup (Tab. 6) a processing model was set up to get the counts of the peak integrals for the elements listed in table 6. A χ^2 value and an error range for each peak integral and a χ^2 value for the whole spectra gives a statistical quality control for peak fitting.

ERROR EVALUATION

Source Stability

Stable measurement conditions are highly important for downcore investigations of semi-quantitative changes in element concentrations. The energy-level settings for the X-ray source were, therefore, not changed through the entire ANDRILL measuring phase. Nevertheless, we detected a drop of the rhodium peak counts (setting A) of about 20% between 297.46 and 444.55 mbsf. The X-ray source has a rhodium anode and this could indicate a drop in bremsstrahlung emission during that period. This drop in peak counts is also visible in Sn (-20%). Some of the core sections were measured again after rhodium was back at its initial level and show normal values. These double measurements will be used to correct for the intensity drop. Other variations of the rhodium peak counts downcore (Fig. 9) could possibly be interpreted as an effect of mass attenuation coefficients.

All elements show scattering around a mean value downcore, partly related to counting statistics with the detector and partly due to core heterogeneity. These variations are different for each element and even two adjacent measurements could read significantly different values of elemental composition and peak counts.

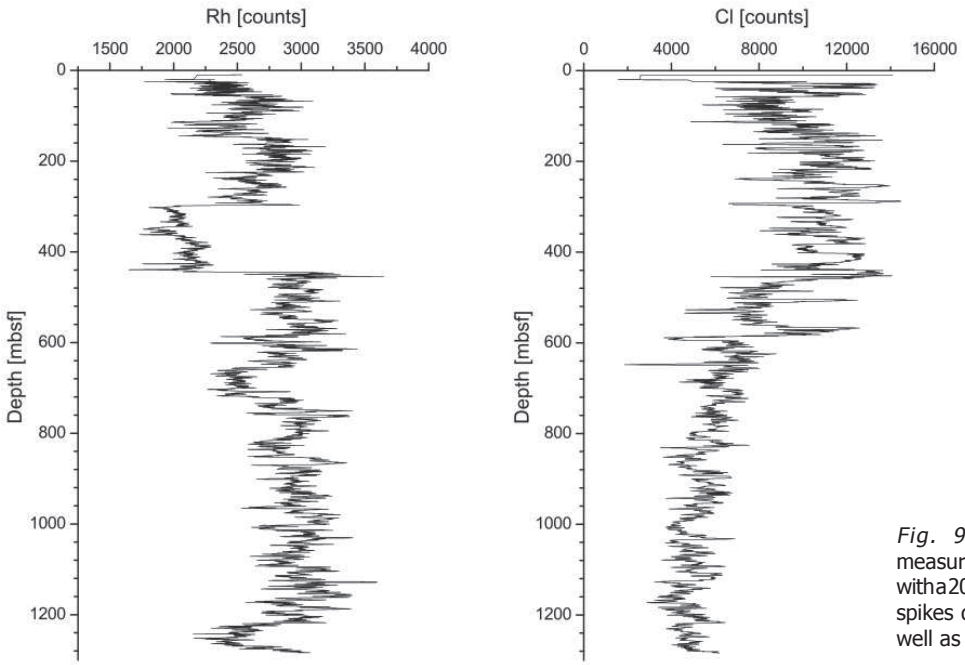

Fig. 9 – Rh and Cl downcore measurements. Data were smoothed with a 20-points running mean to diminish spikes due to measurement errors as well as core heterogeneities.

Adsorption of X-ray Fluorescence by Air

The X-ray fluorescence energy from light elements is low and easily absorbed by air. The core surface was not always smooth due to saw marks or coarser-grained sediment matrix, allowing air below the detector. To correct for the effect of air between the core surface (*i.e.* the covering foil) and the measuring prism, several tests were performed before the actual AND-1B measuring phase. Ar was shown to be the only element that could be detected in air and was thus used for the corrections. Standard materials JB1, JBG1, JR1, and SARM4 (NIST, National Institute of Standards and Technology) were measured 10 times each setting with increasing air distances between the measuring unit and the sample in the XRF scanner.

Absorption by the Ultralene Foil and Water Film between Foil and Sediment Surface

The X-ray fluorescence has to pass through the 4 µm SPEXCerti Prep Ultralene® film that covered the sediment surface to protect the core and the measuring prism, the bottom of the prism and the detector window of the prism. The fluorescence transmission mainly of the lighter elements such as Al, Si, and Cl is reduced by 88%, 92%, and 98%, respectively, per foil. Heavier elements are not affected (Tjallingii et al. 2007).

Cohesive and adhesive properties of the interstitial water forms a thin water film directly below the Ultralene® foil covering the core surface. The water film between the foil and the sediment surface further affects these data (Kido et al. 2006; Tjallingii et al. 2007). Tjallingij et al. (2007) used the Cl counts as a proxy for interstitial water, assuming the only source for Cl is the marine water. They compared the Al and Si element intensity ratios of wet and dry sample measurements to the Cl intensities. A correction following Tjallingij et al. (2007) will be carried out in the home lab.

IMAGE COLLECTION AND VISUAL REFLECTANCE

Line Scan

A 3CCD high-speed colour line-scan camera CV-L105 is integrated in the XRF Core Scanner system and was used for colour scanning. The camera uses a diachronic colour interference filter and three line-scan device arrays (2 048 pixels each) to continuously record the three red-green-blue (RGB) colour channels. While calibration was carried out with the aperture set to 16, scanning was done with the aperture set to 11. Image scans were done with a resolution of 152 scan lines per centimetre in vertical and 2 048 pixels in horizontal direction. The split core was scanned in 1 metre-long sections and the images were saved in different image formats (.bmp and .jpg). Profiles for each RGB channel (red-green-blue) as well as L* (lightness), a* (redness), and b* (yellowness) values were produced by averaging pixels perpendicular to the core in a rectangle along the central core axis and the resulting values were saved as ASCII files. The rectangle was adjusted for each core individually in order to avoid measuring points on the liner or over missing core parts.

Spectrophotometer

Quantitative measurements of diffuse spectral colour reflectance, integrated over an area with a spot size of 1 cm in diameter, were carried out with a handheld Minolta CM-2002 spectrophotometer (Minolta Camera Co., Osaka, Japan). A precise documentation of the camera settings is given in Balsam et al. (1998). The spacing of measurements was mostly set to 2 cm, but increased to 1 cm in case of high variable lithologies and decreased to

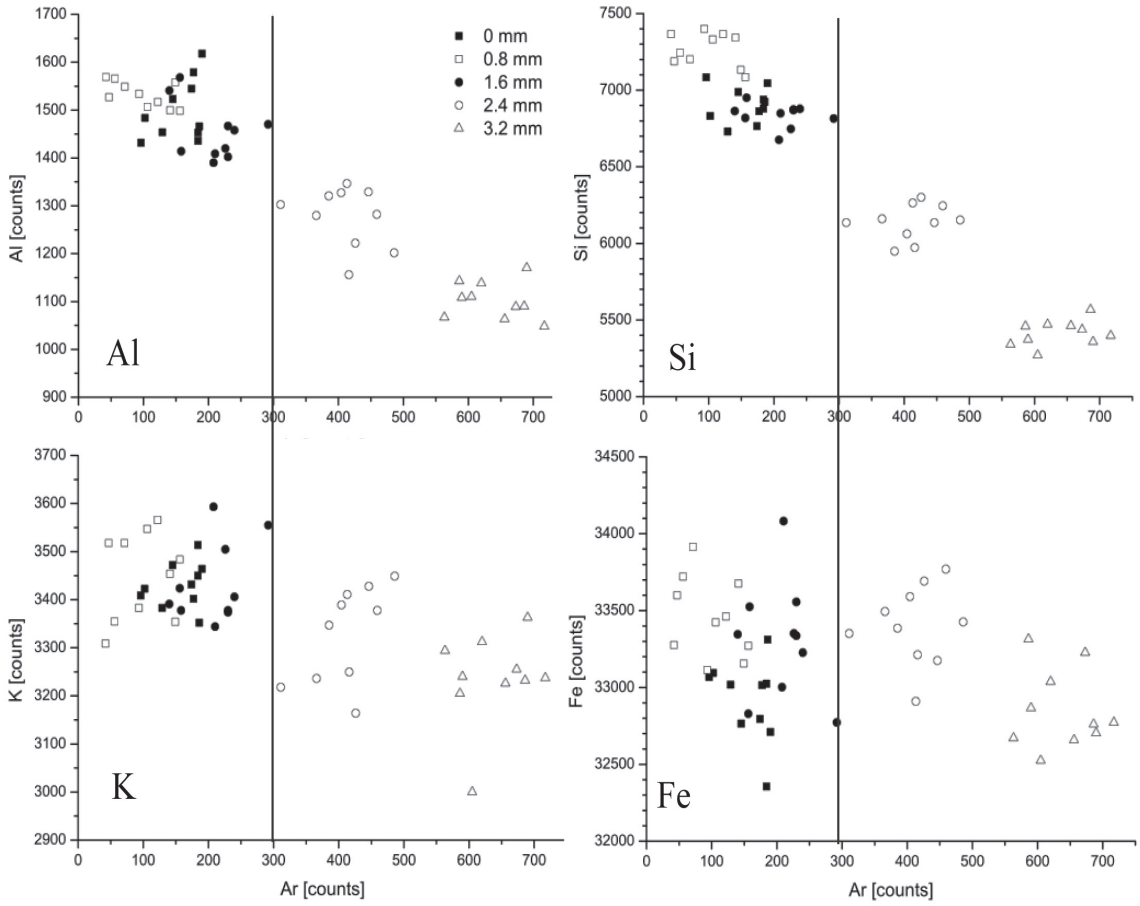

Fig. 10 – Ar versus Al, Si, K, and Fe counts. The Al and Si peak area counts show a clear decrease to lower values above 300 Ar peak counts. Fe does not show this trend.

5 cm in cores with homogenous colours. A clear plastic wrap covered the split core surface to avoid contamination. The calibration was done according to Minolta CM-2002 user's manual (Minolta Camera Co.Minolta Camera Co. 1991). Each data set contains the depth in core-run (that has to be converted to depth in core), CIE-lab L*a*b*, Munsell (hue, value, chroma), the readings from each channel between 400 and 700 nm with 10 nm resolution (30 values), and CIE 1931 norm colour values XYZ. Measurements were carried out down to 984.87 mbsf only because of instrument malfunction. The data were saved to ASCII files individually for each core-run, and down to 200 mbsf they are processed and depth-correlated.

Single Samples

Discrete samples were taken at about 1 per m down the length of the core in order to calibrate the relative element intensity counts received from the XRF core scanner and to do further geochemical analyses. These samples were freeze-dried, and cracked, and gravel (>2 mm) removed. The cleaned sample was then ground to an analytical powder and measured as a discrete sample with the same XRF core scanner in the home laboratory. These measurements were then compared to the measurements made on the wet core. This procedure allows an estimate to be made of the effect of absorption by the occurring water film between the core surface and the covering SPEXCerti Prep Ultralene® film (refer to 'Absorption by the Ultralene Foil' section above). An absorption effect mainly was visible for the light elements such as Al and Si.

In the future, discrete samples will be measured by means of ICP-MS and conventional XRF to quantify the relative measurements of the XRF core scanner.

RESULTS AND DISCUSSION

Ar Correction

A first quality check of the data set was carried out by using argon (Ar) as an indicator of air occurring between the helium flushed prism and the core surface. A threshold of 300 Ar counts was determined as the critical limit for this test by plotting the element counts of the standard material against the Ar counts. Data points related to the lighter elements Al, Si, S, P, K, Ca, and Ti had a decrease in total counts above this threshold. As shown in figure 10, the slit distance of 0 and 0.8 mm had no clear effect on the detection of the element fluorescence. All lighter elements with Ar counts higher than 300 (*i.e. c.* 25% of the measurements) were removed.

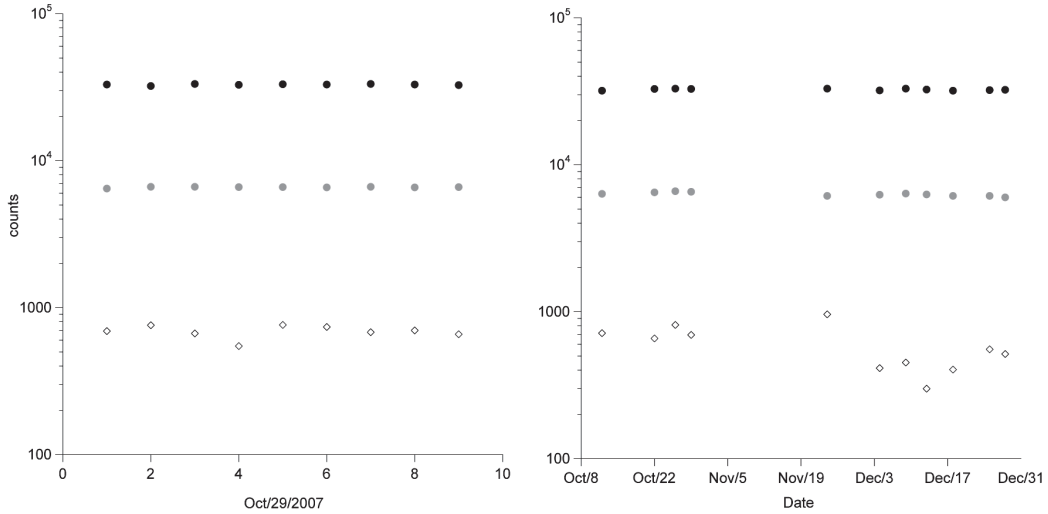

Fig. 11 – Detected total counts for the elements Si (grey), Fe (black), and Cl (rhombi). (A) Intensities at 29 October 2006; (B) Intensities measured from 28 October until 28 December 2006.

Heavier elements did not show this effect according to their higher X-ray fluorescence energy.

Measured Standard Reference Material over Time

Standard reference material was used to estimate instrument drift over time by testing them with the XRF core scanner at regular intervals during the measurement process. These counts are shown for repeated measurements at one date and for measurements for the whole data acquisition phase (Fig. 11). The selected Fe and Si data show no variations; however, a decrease in intensities for the element Cl was detected after the 19 November 2006; standard deviations of each element show the same trend (Tab. 7). Standard deviation counts of Si and Cl increased over the drilling period but a student t-test shows no significant difference between the counts before the 3 December 2006 and after that date.

Source Stability

A loss of X-ray tube excitation during first-run measurements between 297.46 and 444.55 mbsf was detected by a drop in total counts of 20% for the element rhodium (Rh), which represents the material of the X-ray anode. Stable measurements, however, are highly important for high-resolution element profiles downcore. An effect of this energy loss was also detected in Ba, Sn, Ag, and Zr.

To correct these data, parts of specific core sections were re-measured (368.65–376.55 mbsf, 410.60–419.50 mbsf and 434.60–444.85 mbsf). The largest differences between the first and the repeated measurements were in elemental counts from Sn and Ag at about 8% higher, but as the Sn peak is on the flank of the Ag peak, both could have been generated by the Ag-containing beam collimator of the detector. Zr showed only slight variations between the two measurements.

The initial element values were corrected using values determined from both the initial and the

Tab. 7 - Means and standard deviations of measurements of standard reference material (SARM4) on 29 October 2006, and measurements from 22 October to 28 December 2006.

	10 times repeated measurements		*Measurements over time*	
	mean	standard deviation	mean	standard deviation
Si	6598	57	6304	197
Fe	32928	326	32537	446
Cl	548	65	589	198

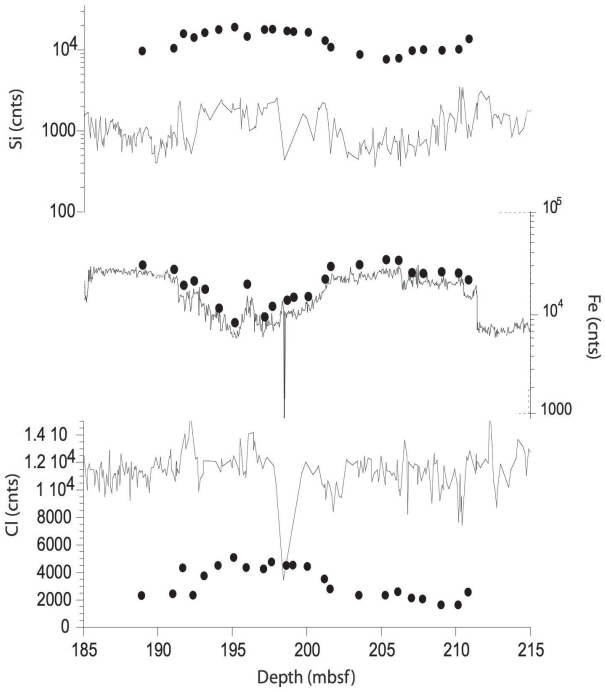

Fig. 12 – Comparison between wet core measurements (line) and discrete dry powder samples (dots) for the elements Si, Fe, and Cl. Intensities of dry powder are much higher for Si and slightly increased for Fe. The measured counts for Cl are decreased in most dry samples.

repeated measurements. Linear regression was used for all elements except Sn for which the mean offset value was calculated. Stable measurements are highly important for downcore investigations of semi-quantitative changes in element concentrations.

Wet Continuous Versus Discrete Dry Powder Measurements

Comparisons between wet core and dry powder measurements (Fig. 12) show variations between 10% for the elements with higher atomic number and up to 200% for the lighter elements like Si and Al. Absorption of X-ray fluorescence by water was described in the study of Tjallingii et al. (2007). They measured wet sediment cores on the split core surface and dried discrete powder samples of the same core to determine the transmission related to physical properties. They estimated the water content by using the measured Cl intensities.

Discrepancies between wet core measurements and dry sample measurements are demonstrated on a selected core section with counts of the elements Si, Fe, and Cl (Fig. 13). Intensities for Si show the largest difference between dry and wet samples, with increased values in the dry samples. Values for Fe show only a slight increase. In contrast, decreased values were measured for all dry powder samples for the element Cl. These elements were chosen as examples here, because they indicate different environments and should be affected in

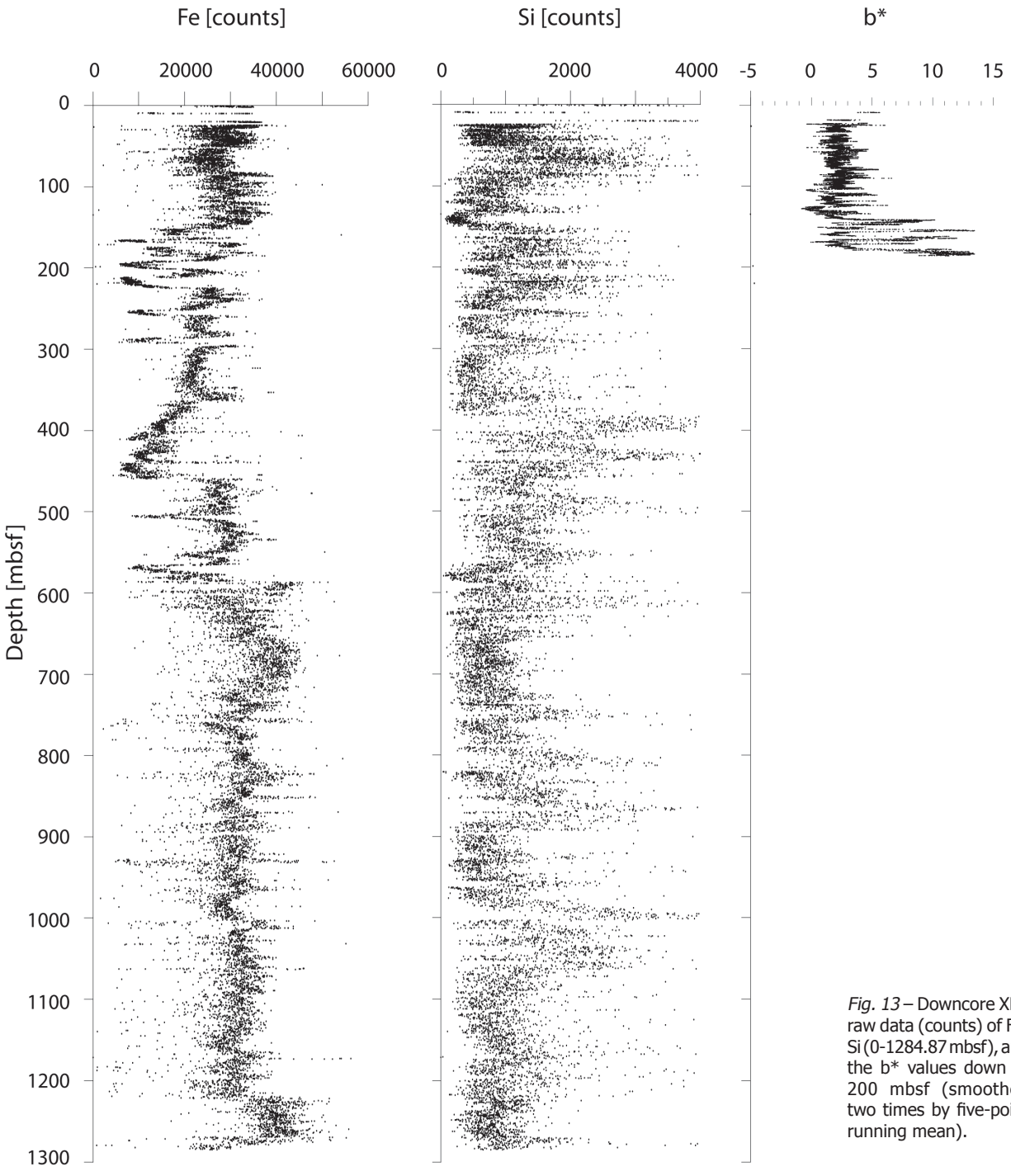

Fig. 13 – Downcore XRF raw data (counts) of Fe, Si (0-1284.87 mbsf), and the b* values down to 200 mbsf (smoothed two times by five-point running mean).

a different way by the interstitial water between the core surface and the foil. The higher intensities in the wet core are related to artificially elevated salty pore-water content. Cohesive and adhesive properties of the interstitial water form this thin water layer below the Ultralene® film and cause higher element intensities of salt ions in the wet core. Elements other than those of sea salt showed a decrease in values perhaps because the water and ions absorb their X-ray fluorescence.

Core Characterisation

A rhythmic pattern in element concentration that corresponds to the changes in the lithologies is evident downcore. These variations are also reflected in the chemical data as well as in the CIE-lab b* values of the spectrophotometer measurements. To demonstrate this pattern, measured values of Si and Fe, and the b* colour data (smoothed twice using a 5-point moving average), were plotted versus core depth (Fig. 13). Maximum values in Si between 150 and 300 mbsf correspond to minima in Fe and maxima in b* and are clearly related to sediments rich in diatoms (diatomites) that were deposited during open-water conditions. Diamictites deposited near the ice sheet have minimum values of Si and b* whereas values for Fe are at their maximum. Some parts of the diamictites have high Si values thus this element is not a consistent indicator of this facies.

Conclusions and Outlook

The high-resolution geochemical data set for AND-1B core provides an outstanding dataset to assess rapid palaeoclimatic changes in the Antarctic. To ensure the quality of the data collected on-ice, various corrections will be carried out for all core sections and all of the discrete samples need to be analysed by using ICP-MS and XRF analysers for calibration of the XRF core-scanner measurements.

CARBONATE GEOCHEMISTRY

Carbonate deposits are used in the AND-1 cores to contribute to a better understanding of palaeoclimatic and palaeoenvironmental conditions in the McMurdo Sound area. Samples available for a geochemical and isotopic characterisation of carbonate deposits and bulk sediment in the AND-1 cores include those from core trimmings, samples remaining from porosity and the squeeze-cake analyses, and samples collected at particular horizons such as rinds, cements, and vein fillings. Twenty-tree thin sections were also made of some samples to understand cementation and fabric patterns.

Sub-samples of those collected for porosity were ground into powders in an agate mortar and their $\delta^{13}C$ and $\delta^{18}O$ composition determined using the FISONS Prism in the Stable Isotope Labatory at University of California-Santa Cruz. Repeat measurements (N = 5) of an internal standard averaged -1.61 per mil with a standard deviation of 0.036 per mil.

Initial results of this work are promising for being able to reconstruct palaeoclimatic and palaeoenvironmental changes (Fig. 14). The profile of core AND1-B shows large variability in $\delta^{13}C$ (-1.0 to -7.3 per mil) and $\delta^{18}O$ (-2 to -13.5 per mil) associated with major glacial/interglacial changes. Most $\delta^{18}O$ excursions to more positive values correspond to core intervals containing diatomites. For example, the $\delta^{18}O$ excursion at 80 mbsf is directly above a diatom-rich formation (86.92–97.08 mbsf) that may be associated with the Marine Isotope Stage 31 (1.07 Ma). Furthermore, the $\delta^{18}O$ excursion at *c.* 400 mbsf correlates with the thickest diatomite interval (377 to 459 mbsf).

The interval below *c.* 800 mbsf shows less variability in $\delta^{13}C$ and $\delta^{18}O$. In this interval pyritisation occurs and it is possible that climatic and environmental signals are smoothed out or overprinted by diagenetic processes.

PORE-WATER GEOCHEMISTRY

Eighty-three pore water samples were collected from 89 sediment samples using a titanium pore-water

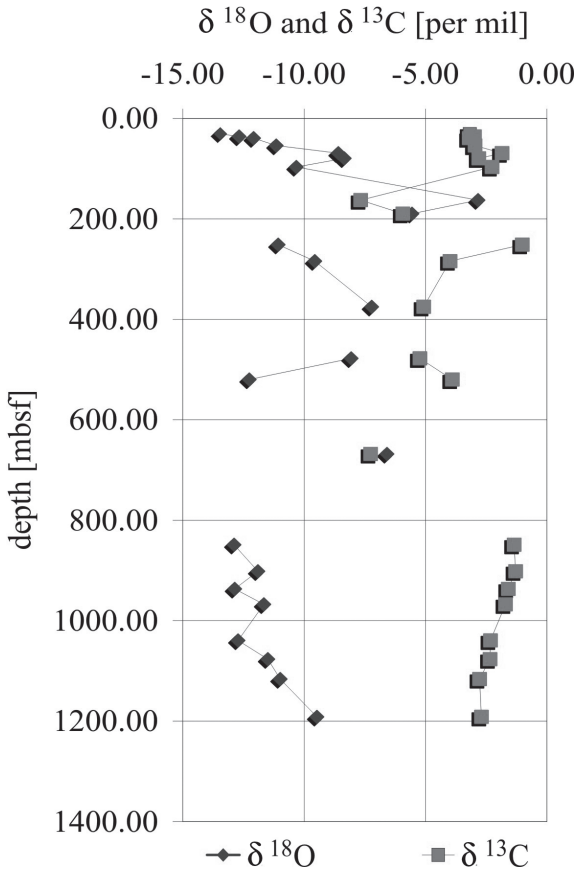

Fig. 14 – $\delta^{13}C$ and $\delta^{18}O$ composition of carbonate in bulk sediment from the AND-1B core.

squeezer and Rhizon-tube samplers. Prior to rotary drilling, several soft-sediment cores were acquired using a gravity corer from the Alfred Wegener Institute (AWI) in Germany (for details, see Dunbar et al. this volume). Of the 83 pore water samples, 28 came from the AND-1A and AND-1B cores.

SOFT-SEDIMENT SAMPLING

The soft sediment (SS) sampling was conducted in conjunction with the microbiology group using the AWI gravity corer (samples labelled 'GC') and from push cores using the ANDRILL rig push-coring device (samples labelled 'PU'). (See Dunbar et al. this volume for details). Pore-water samples were acquired from five of the eight GC and two of the three PU soft-sediment cores. The scientific party involved in this sampling included Gavin Dunbar, Kevin Mandernack, Matt Olney, Chieh Peng, Ross Powell, and Stefan Vogel. Pore water was extracted from 5 cm-thick full-round sections collected in alternating sequence with microbiological sampling using a titanium pore-water squeezer on loan from the Ocean Drilling Program (ODP). ODP pore-water extraction procedures were adapted to the ANDRILL set-up. Rhizon samplers were used to extract pore water from SS-07 GC and SS-09 push cores.

After recovery of the soft-sediment cores, the cores were capped and transferred to the drill-site laboratory (lab). Cores were then extracted in 5 cm increments from their liners while in a laminar-flow hood. Pore-water samples were sealed and capped immediately and transferred to the Crary Lab at McMurdo Station within hours.

In the Crary Lab, the outside of each sample was cleaned by cutting away a *c.* 1 cm-thick rim. The remaining clean inner core of the sample was then transferred into the titanium squeezer. This procedure followed ODP pore-water extraction protocols as instructed by Chieh Peng (ODP technician; see Manheim & Sayles [1974] for details on the squeezer). The squeezer was transferred into a hydraulic press and a maximum pressure of 20 000 to 30 000 lbs was applied and reached after about 1 to 1.5 hr. After an initial consolidation phase with applied pressures of *c.* 5000 lbs the pressure was manually increased in steps of 2 000 to 3 000 lbs. All pore-water samples were collected with 50 ml plastic syringes after the water had passed through a Whatman no.1 filter at the bottom of the squeezer. All syringes were acid cleaned with 10% HCl prior to use.

MAIN CORE SAMPLING

During the main drilling phase porewater samples were extracted from 10 to 20 cm-thick and 20 cm-thick half round cores of PQ and HQ diameter, respectively, and 20 cm-thick full round cores of NQ diameter. The sample for extracting pore-water was taken directly after the core was split and it was then transferred into the lab where it was either stored for a few hours in the refrigerator at 4°C or immediately prepared for squeezing. The outer 0.5 to 1 cm rim was either cut or chiselled away to prevent drill fluid or cutting fluid contamination.

With an increase in consolidation and decrease in porosity with depth, the time to extract the pore water increased from *c.* 1 hour on the soft-sediment samples to 12 to *c.* 24 hours on PQ and HQ-core samples. The maximum pressure applied to the PQ, HQ, and NQ samples averaged 40 000 to 45 000 lbs and they went through an initial consolidation phase applying increasing pressure in 5000 to 10 000 lbs increments similar to the SS extraction. Thereafter the pressure was increased in *c.* 2000 to 3000 lbs increments about once every one to two hours. The last sample (1266 mbsf) was pressed for 48 hours; however, no water could be extracted despite increasing the pressure to 50 000 lbs. The limit for extracting pore water with our set-up was ~26% water-content for highly consolidated glacial diamictite and 32% for highly cemented sand and mudstones.

Water content was measured on about 5 to 20 g of sediment taken from sample trimmings. The sample was weighed and dried in a convection oven at 105°C overnight. Repeated measurement of the dry weight after several days in the oven gave an overall accuracy of the measurement of 1%. By measuring the water content prior to squeezing, it was possible to return two samples to the curators because it was determined their water content was too low for squeezing. They could then be made available for future work, instead of having their structural integrity destroyed.

Pore-water extraction was not fast enough to follow the originally anticipated sampling interval of *c.* 30 m without backing-up samples. This led initially to a decrease in sample density by larger sample intervals, but storing backed-up vacuum-sealed samples in a refrigerator may provide a solution and optimisation of time. The stored samples would complement the profile with crucial data, which otherwise would never be obtained. Availability of a second automated hydraulic press would also allow processing of more samples.

RHIZON SAMPLING PROCEDURES

Rhizon sampling is a method to extract pore water, which does not destroy the acquired sediment core and causes only minimal disturbance of the core beyond dewatering. The Rhizon sampler consists of a membrane filter attached to tygon tubing, which is inserted through a small hole in the core liner. The inserted sampler is then either attached to a syringe or a glass vacuum tube, and pore water is extracted using the suction created by the applied vacuum. Each Rhizon sampler was acid cleaned prior to use with 30 ml of 1% HCl and carefully rinsed with Milli-Q water.

PORE-WATER SAMPLE HANDLING AND ON-ICE MEASUREMENTS

All samples were filtered after collection through a 0.2 μm nylon membrane filter into acid washed HDPE plastic vials. Aliquots for individual analytical work were then dispensed into 4 ml acid-cleaned HDPE vials for elemental geochemistry, on-ice and on-site work, and glass vials for stable isotope ($\delta^{18}O$, δD), dissolved inorganic carbon (DIC), $\delta^{13}C$ on DIC samples. A 2 ml fraction of sample was preserved with 10 μl chloroform for measurements of DIC (J. Priscu personal communication 2006), and *c.* 4 ml of sample was preserved using *c.* 30 mg mercury chloride for determining the $\delta^{13}C$ on the DIC (*cf.* Torres et al. 2005). When sufficient sample quantity was available 2 to 4 ml were allocated for measuring $\delta^{34}S$ and $\delta^{18}O$ on dissolved sulfate. These samples were preserved using zinc acetate (Blake et al. 2006) that precipitates out dissolved sulfides.

Larger-volume samples had 2 to 3 ml measured for pH, alkalinity, and electrical conductivity immediately after acquisition. First, pH was measured directly after inserting a pH probe, then again after a certain time of equilibration, when the drift in the pH reading was less than pH 0.002. This pH equilibration was typically reached after 10 to 30 minutes. After the pH measurements, samples were titrated with 1 M HCl to determine alkalinity using Gran titration with a Beckman futura micro-combination pH electrode and a Metrohm auto-titrator. In addition, major cation and anion concentrations were measured on-ice using ion-chromatography three times during the season.

For better calibration, all samples were again measured at the end of the season for anions, and all except samples AND-1-004 to 008-GC and those from cores AND-1-007-GC and AND-1-009-PU were measured for cations. Cation data for these samples came from an IC run made on 2 December 2006 (see Dunbar et al. this volume for discussion). Due to low sample volume, the electrical conductivity measurement was done on 2 ml of sample in a graduated HDPE plastic cylinder. The measurement needs to be adjusted to open-beaker measurements due to proximity of the cylinder wall on measurements. Ammonium and chloride concentration were also measured on-ice following ODP lab procedures (Gieskes et al. 1991). Ammonium was measured on a Shimadzu 2501 spectrometer.

All on-ice and off-ice samples were refrigerated at 4°C and stored in the McMurdo lab. Samples were shipped off-ice in specialised cooling containers; arrival temperatures at Port Hueneme ranged from 12.1 to 14.0°C, whereas when they arrived at University of California-Santa Cruz temperatures ranged from 7.1 to 9.3°C. A total of 55 drill-fluid samples were collected, one on each day of drilling operations, to assess the potential of drill-fluid contamination. One drill-fluid sample, collected for microbiological work, was frozen immediately after arrival in the lab at McMurdo Station, approximately 3 to 4 hours after collection.

DRILL FLUID CONTAMINATION

The potential for drill-fluid contamination of the collected pore-water samples can be assessed using the potassium concentration. Drill fluid consisted mainly of seawater mixed with potassium chloride and some other densifiers that were used in only minor amounts. Chloride concentrations in most pore-water samples are on the order of chloride concentration in the drill fluid, so that chloride does not provide a good measure to detect drill-fluid contamination. Two pore-water samples from highly porous volcanic sandstones at 112 and 138 mbsf have a noticeably higher viscosity than other samples that had problems penetrating the 0.2 μm filters. Their high potassium concentrations at *c.* 20 times that of

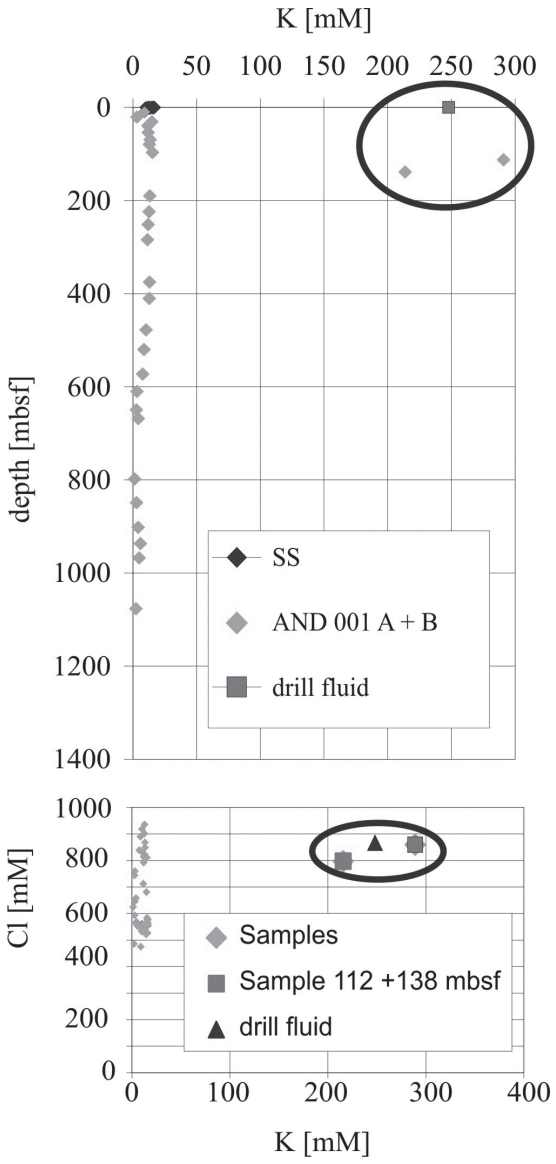

Fig. 15 – Two pore-water samples from a depth of 112 mbsf and 137 mbsf show a clear signal of drill-fluid contamination. Potassium concentrations in these two samples (circle) are similar to concentrations in drill fluid (square) (upper panel), whereas chloride concentration are indistinguishable (lower panel).

other pore-water samples (see Fig. 15) is similar to that of the drill fluid indicating it had penetrated the porous rock and contaminated these samples. This geochemical signature of drill-fluid contamination is absent in all other samples. Even small amounts of drill-fluid contamination (<1%) would show a clear signature in samples with elemental concentrations significantly lower than seawater. We are therefore confident that having removed the outer 0.5 to 1 cm of the squeezed cores, all pore-water samples are uncontaminated with the exception of the two porous volcanic sandstones.

ACCURACY OF CHEMICAL ANALYSIS

The accuracy of our geochemical measurements can be assessed using electro-neutrality (E.N. [%]) assessing the charge balance of the measured cations and anions (*cf.* Appelo and Postma, 1996).

$$\text{E.N. [\%]} = (\text{Sum cations} + \text{Sum anions}) / (\text{Sum cations} - \text{Sum anions}) \times 100$$

with cations and anions being expressed in meq/l using their appropriate charge sign (cations positive, anions negative).

The calculated electro-neutrality of the suite of pore-water samples is good, with an average of 0.75% and standard deviation of 1.00%. However, electro-neutrality of samples from cores AND-1-007-GC and AND-1-009-PU, and samples AND-1-004 to 008-GC average 8.81% with standard deviation of 1.95% (see Tab. 8) and may not be reliable. Ion chromatography measurements of these latter samples were corrected to account for analytical drift during individual runs, but they continued to have a low reproducibility. However, reproducibility of the remaining samples is excellent and therefore data interpretation focuses on the AND-1A and AND-1B profile. Ion chromatography measurements were corrected for analytical drift during individual runs. The reproducibility of these analyses was determined by repeat measurements of a standard with concentrations corresponding to a *c.* 1:100 sample dilution. Reproducibility for different ions is: F^- ±2%-7%, Cl^- ±2%, Br^- ±1%-2%, SO_4^{2-} ±2%-3%, Li^+ ±13%-22%, Na^+ ±2%-6%, K^+ ±4%-6%, Mg^{2+} ±2%-5%, Ca^{2+} ±2%-6%. The higher values (anions ±2%-7% and cations ±5%-13%) correspond to samples from AND-1-007-GC, AND-1-009-PU and AND-1-00 to 008-GC. NO_2^-, NO_3^-, and PO_4^{3-} concentrations are close to or below the detection limits and are therefore not considered.

The reproducibility of Cl^- was also tested using silver nitrate titration (± 1.8%), and alkalinity (± 4.4%) was determined by repeat measurements of IAPSO standard seawater. The reproducibility of NH_4^+ (colourimetric) was ±0.9 to 3.5 µM corresponding to ± 9% at *c.* 10 µM and ± 0.1% at *c.* 3 500 µM.

INITIAL RESULTS AND DISCUSSION

Cation concentrations above 20 mbsf decrease downcore (Fig. 16A), whereas anion concentrations

Tab. 8 - Reproducibility of measurements in pore-water analysis.

IC	F	Cl	Br	SO_4		NO_2	NO_3	PO_4
run 1230A								
average [mM]	0.057	26.179	0.127	1.043		0.086	0.031	0.021
N								
stdev	0.004	0.639	0.002	0.021		0.005	0.001	0.002
stdev/avg	7.4%	2.4%	1.6%	2.0%		5%	3%	11%
run 1231A								
average [mM]	0.053	25.752	0.122	1.080		0.088	0.030	0.019
N								
stdev	0.001	0.495	0.002	0.028		0.004	0.000	0.003
stdev/avg	2.4%	1.9%	1.4%	2.6%		5%	1%	14%

IC	Li	Na	K	Mg	Ca
run 0101C					
average [mM]	0.024	29.180	0.968	7.455	0.921
N	11	5			
stdev	0.005	0.638	0.037	0.143	0.020
stdev/average	22%	2.2%	3.8%	1.9%	2.2%
run 1202C					
average [mM]	0.037	438.574	9.844	49.982	9.889
N					
stdev	0.005	24.487	0,621	2.500	0.547
stdev/average	13%	5.6%	6.3%	5.0%	5.5%

	Cl tiration	Alkalinity		NH_4^+	NH_4^+
average [mM]	558.18	2.48		0.001	3.225
N	11	5		4	6
stdev	0.982	0.109		0.00009	0.0035
stdev/average	0.18%	4.4%		9%	0.1%

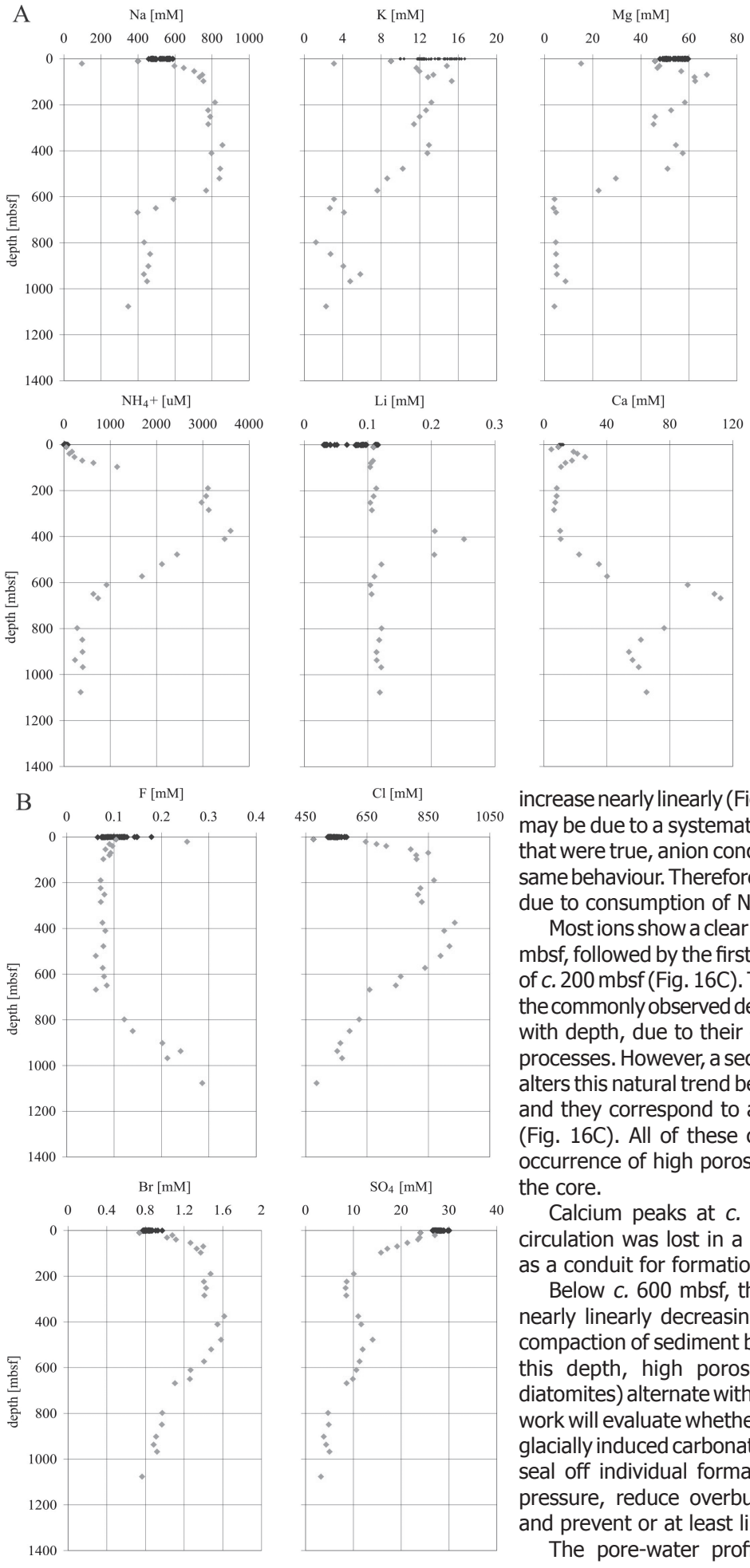

Fig. 16 – Geochemistry of pore water in the AND-1 cores. (A) cation concentration profiles (Na, K, Mg, NH4+, Li, Ca); (B) anion concentration profiles (F, Cl, Br, SO_4).

increase nearly linearly (Fig. 16B). The cation decrease may be due to a systematic dilution error; however, if that were true, anion concentrations should show the same behaviour. Therefore, this decrease is most likely due to consumption of Na, K, Mg, and Ca cations.

Most ions show a clear peak between *c.* 60 and 100 mbsf, followed by the first peak in alkalinity at a depth of *c.* 200 mbsf (Fig. 16C). These peaks are followed by the commonly observed decrease in ion concentrations with depth, due to their consumption by diagenetic processes. However, a second concentration increase alters this natural trend between *c.* 380 and 650 mbsf and they correspond to a stepwise increase in $\delta^{18}O$ (Fig. 16C). All of these changes correlate with the occurrence of high porosity diatomites (Fig. 16C) in the core.

Calcium peaks at *c.* 668 mbsf where drill-fluid circulation was lost in a formation that could serve as a conduit for formation water.

Below *c.* 600 mbsf, the porosity profile shows a nearly linearly decreasing trend, related to natural compaction of sediment by lithostatic loading. Above this depth, high porosity layers (predominantly diatomites) alternate with low porosity layers. Further work will evaluate whether this pattern is the result of glacially induced carbonate cementation, which could seal off individual formations, increase pore-water pressure, reduce overburden-induced compaction, and prevent or at least limit vertical fluid migration.

The pore-water profile shows a very unusual

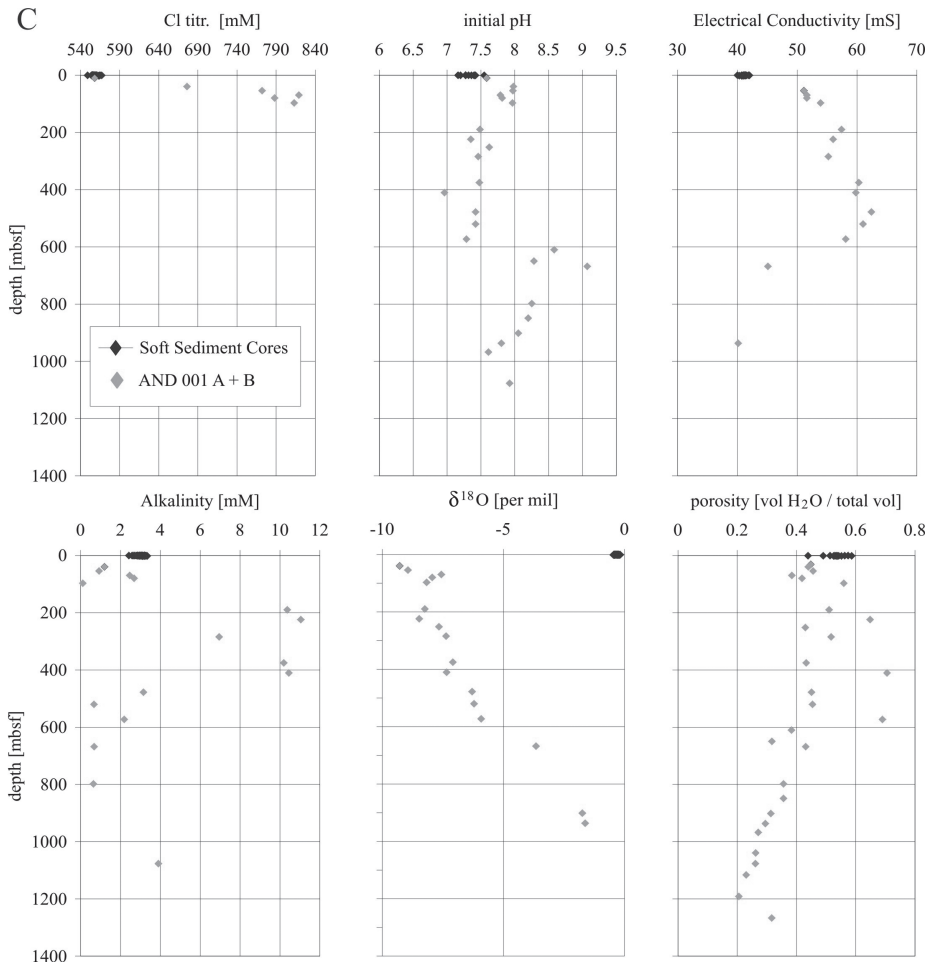

Fig. 16 – Continued. (C) Cl by silver nitrate titration, pH , electrical conductivity, alkalinity, $\delta^{18}O$, and porosity profile.

geochemical behaviour and detailed interpretation requires more detailed study to assess the relative importance of different processes: (i) regional sedimentary diagenetic, (ii) volcanic, and (iii) glacial and subglacial.

Acknowledgements– The ANDRILL project is a multinational collaboration between the Antarctic programmes of Germany, Italy, New Zealand and the United States. Antarctica New Zealand is the project operator and developed the drilling system in collaboration with Alex Pyne at Victoria University of Wellington and Webster Drilling and Enterprises Ltd. Antarctica New Zealand supported the drilling team at Scott Base; Raytheon Polar Services Corporation supported the science team at McMurdo Station and the Crary Science and Engineering Laboratory. The ANDRILL Science Management Office at the University of Nebraska-Lincoln provided science planning and operational support. Scientific studies are jointly supported by the US National Science Foundation, NZ Foundation for Research, Science and Technology and the Royal Society of NZ Marsden Fund, the Italian Antarctic Research Programme, the German Research Foundation (DFG) and the Alfred Wegener Institute for Polar and Marine Research. We are all indebted to Brent Pooley (Otago University) for his excellent hard work every day making thin sections. Matteo Cattadori (ARISE) and Sonia Sandroni helped in counting/recounting clasts on and off ice, respectively. $\delta^{13}C$ and $\delta^{18}O$ on bulk carbonates were measured by Dyke Andreasen in the stable isotope at University of California-Santa Cruz. Aside from the support through ARISE participants Luann Dahlman and Betty Trummel, Stefan Vogel would like to thank Chieh Peng (Integrated Ocean Drilling Program [IODP]) and Rene Estelle (McMurdo staff volunteer) for their help with the pore-water work. We also thank Kathy Welch and the Long-Term Ecological Research (LTER) group, for support and for providing access to their ion chromatograph at McMurdo Station.

REFERENCES

Allibone A.H., 1992. Low Pressure/High Temperature Metamorphism of Koettlitz Group Schists in the Taylor Valley and Ferrar Glacier Regions. *N.Z. J. Geol. Geophys.,* **35**, 115–127.

Allibone A. H., Cox S.C., Graham I.J., Smillie R.W., Johnstone R.D., Ellery S.G., & Palmer K., 1993b. Granitoids of the Dry Valleys Area, Southern Victoria Land, Antarctica: Plutons, Field Relationships, and Isotopic Dating. *N.Z. J. Geol. Geophys.,* **36**, 281–297.

Allibone A.H., Cox S.C., & Smillie R.W., 1993a. Granitoids of the Dry Valleys Area, Southern Victoria Land: Geochemistry and Evolution along the Early Paleozoic Antarctic Craton Margin. *N.Z. J. Geol. Geophys.,* **36**, 281–297.

Appelo C.A.J. & Postma D., 1996. *Geochemistry, Groundwater and Pollution*. A.A. Balkema, Rotterdam.

Armienti P., Tamponi M., & Pompilio M., 2001. Sand Provenance from Major and Trace Element Analyses of Bulk Rock and Sand Grains from CRP2/2A, Victoria Land Basin, Antarctica. *Terra Antartica*, **8**, 569–582.

Balsam W.L., Deaton B.C., & Damuth J.E., 1998. The Effects of Water Content on Diffuse Reflectance Spectrophotometry Studies of Deep-Sea Sediment Cores. *Marine Geology,* **149**, 177–189.

Barrett P.J., Carter L., Dunbar G.B., Dunker E., Giorgetti G., Harper M.A., McKay R.M., Niessen F., Nixdorf U., Pyne A.R., Riesselman C., Robinson N., Hollis C., & Strong C.P., 2005. *Oceanography*

and Sedimentation beneath the McMurdo/Ross Ice Shelf in Windless Bight, Antarctica. Antarctic Data Series 25, Victoria University Antarctic Research Centre, 100 p.

Blake R.E., Surkov A.V., Böttcher M.E., Ferdelman T.G., & Jørgensen B.B., 2006. Oxygen Isotope Composition of Dissolved Sulfate in Deep-Sea Sediments: Eastern Equatorial Pacific Ocean. In: Jørgensen B.B., D'Hondt S.L., & Miller, D.J. (eds.), *Proceedings of the Ocean Drilling Program, Scientific Results,* College Station, TX (Ocean Drilling Program), **201**, 1–23 doi:10.2973/odp.proc.sr.201.116.2006.

Cape Roberts Science Team, 1998a. Background to CRP-1, Cape Roberts Project, Antarctica. *Terra Antartica*, **5**, 1–30.

Cape Roberts Science Team, 1998b. Quaternary Strata in CRP-1, Cape Roberts Project, Antarctica. *Terra Antartica*, **5**, 31–62.

Cape Roberts Science Team, 1998c. Miocene Strata in CRP-1, Cape Roberts Project, Antarctica. *Terra Antartica,* **5**, 63–124.

Cape Roberts Science Team, 1998d. Summary Results from CRP-1, Cape Roberts Project, Antarctica. *Terra Antartica*, **5**, 125–138.

Cape Roberts Science Team, 1999. Studies from Cape Roberts Project. Initial Report on CRP-2/2A, Ross Sea, Antarctica. *Terra Antartica*, **6**, 1–173.

Cape Roberts Science Team, 2000. Studies from Cape Roberts Project. Initial Report on CRP-3, Ross Sea, Antarctica. *Terra Antartica*, **7**, 1–209.

Dunbar G., Niessen F., Vogel S., Tulaczyk S., Mandernack K., Krissek L., Carter L., Cowan E., Wilch T., Peng C., Strong C.P., Scherer R., Sjunneskog C., Winter D., McKay R., Talarico F., Pompilio M., & the MIS-Science Team, this volume. Late-Pleistocene to Holocene Strata from Soft-Sediment Coring at the AND-1B Site, ANDRILL McMurdo Ice Shelf Project, Antarctica. *Terra Antartica*.

Findlay R.H., Skinner D.N.B., & Craw D., 1984. Lithostratigraphy and Structure of the Koettlitz Group, McMurdo Sound, Antarctica. *N.Z. J. Geol. Geophys.,* **27**, 513–536.

Ge L., Lai W., & Lin Y., 2005. Influence of and Correction for Moisture in Rocks, Soils and Sediments on In Situ XRF Analysis. *X-Ray Spectrometry,* **34**, 28–34.

Gieskes, J.M., Toshitaka G., & Brumsack H., 1991. Chemical Methods for Interstitial Water Analysis Aboard Joides Resolution, *ODP Technical Note 15*.

Grindley G.W. & Warren G., 1964. Stratigraphic Nomenclature and Correlation in the Western Part of the Ross Sea. In: Adie R.J. (ed.), *Antarctic Geology*. Amsterdam, North Holland Publishing Co., 314–333.

Gunn B.M. & Warren G., 1962. Geology of Victoria Land between the Mawson and Mulock Glaciers, Antarctica. *N.Z. Geol. Surv.*, **71**.

Hambrey M.J., Barrett P.J., & Robinson P.H., 1989. Stratigraphy. In: Barrett P.J. (ed.), Antarctic Cenozoic history from the CIROS-1 drillhole, McMurdo Sound. *DSIR Bulletin*, **245**, 23–48.

Kido Y., Koshikawa T., & Tada R., 2006. Rapid and Quantitative Major Element Analysis Method for Wet Fine-Grained Sediments using an XRF Microscanner. *Mar. Geol.,* **229**, 209–225.

Kretz R., 1983. Symbols for Rock Forming Minerals. *Am. Mineral.,* **68**, 277–279.

Krissek L., Browne G., Carter L., Cowan E., Dunbar G., McKay R., Naish T., Powell R., Reed J., Wilch T., & the ANDRILL-MIS Science Team, this volume. Sedimentology and Stratigraphy of the AND-1B Core, ANDRILL McMurdo Ice Shelf Project, Antarctica. *Terra Antartica.*

Kyle, P.R., 1981. Mineralogy and Geochemistry of a Basanite to Phonolite Sequence at Hut Point Peninsula, Antarctica, Based on Core from Dry Valley Drilling Project Drillholes 1, 2 and 3. *J. Petrol.*, **22**, 451–500.

Kyle P.R., 1990. A. McMurdo Volcanic Group, Western Ross Embayment. Introduction. In: Le Masurier W.E. & Thomson J.W. (eds.), *Volcanoes of the Antarctic Plate and Southern Oceans*. AGU Antarctic Research Series, **48**, 19–25.

Kyle P.R., Elliot D.H., & Sutter J.F., 1981. Jurassic Ferrar Supergroup Tholeiites from the Transantarctic Mountains, Antarctica, and Their Relationship to the Initial Fragmentation of Gondwana. In: Cresswell, M.M. & Vella, P. (eds.), *Gondwana Five. Fifth International Gondwana Symposium,* 283–287.

Le Maitre R.W. (ed.), 2002. *A Classification of Igneous Rocks and Glossary of Terms. Recommendations of the IUGS Subcomission on the Systematics of Igneous Rocks*. Cambridge University Press, Cambridge, UK.

Manheim F.T. & Sayles F.L., 1974. Composition and Origin of Interstitial Waters of Marine Sediments, Based on Deep Sea Drill Cores. In: Goldberg, E.D. (ed.), *This Sea–Marine Chemistry: Sedimentary Cycle*, vol. 5, Wiley, New York, 527–568.

McIntosh W.C., 2001. $^{40}Ar/^{39}Ar$ Chronology of Tephra and Volcanic Clasts in CRP-2A, Ross Sea, Antarctica. *Terra Antartica,* **7**, 621–630.

Minolta Camera Co., 1991. Spektrophotometer CM-2002 Bedienerhandbuch. In: L. Minolta Camera Co. (ed.), Minolta GmbH, Ahrensburg.

Richter T.O., Van der Gaast S., Koster B., Vaars A., Gieles R., De Stigter H.C., De Haas H., & Van Weering C.E., in press. The Avaatech Core Scanner: Technical Description and Applications to NE Atlantic Sediments. In: Rothwell R.G. (ed.), *New Ways of looking at Sediment Core and Core Data*. Geological Society Special Publication, London.

Roehl U. & Abrams L.J., 2000. High-Resolution, Downhole, and Nondestructive Core Measurements from Sites 999 and 1001 in the Caribbean Sea; Application to the Late Paleocene Thermal Maximum. In: Leckie R.M., Sigurdsson H., Acton G.D., & Draper G. (eds.), *Proceedings of the Ocean Drilling Program, Scientific Results*, College Station, TX (Ocean Drilling Program).

Sandroni S. & Talarico F.M., 2001. Petrography and Provenance of Basement Clasts and Clast Variability in CRP-3 Drillcore (Victoria Land Basin, Antarctica). *Terra Antartica*, **8**, 449–467.

Sandroni S. & Talarico F.M., 2004. Petrography and Provenance of Basement Clasts in CIROS-1 Core, McMurdo Sound, Antarctica. *Terra Antartica,* **11**, 93–114.

Sandroni S. & Talarico F.M., 2006. Analysis of Clast Lithologies from CIROS-2 Core, New Harbour, Antarctica - Implications for Ice Flow Directions during Plio-Pleistocene. *Palaeoleogr., Palaeoclim., Palaeoecol.*, **231**, 215–232.

Talarico F. & Sandroni S., 1998. Petrography, Mineral Chemistry and Provenance of Basement Clasts in the CRP-1 Drillcore (Victoria Land Basin, Antarctica). *Terra Antartica,* **5**, 601–610.

Talarico F.M., Sandroni S., Fielding C., & Atkins C., 2000. Variability, Petrography and Provenance of Basement Clasts from CRP-2/2A Drillcore (Victoria Land Basin, Antarctica). *Terra Antartica,* **7**, 529–544.

Tjallingii R., Röhl U., Kölling M., & Bickert T., 2007. Influence of the Water Content on X-ray Fluorescence Core Scanning Measurements in Soft Marine Sediments. *Geochem Geophys Geosys*, **8**, 12.

Torres M.E., Mix A.C., & Rugh W.D., 2005. Precise d13C Analysis of Dissolved Inorganic Carbon in Natural Waters using Automated Headspace Sampling and Continuous-Flow Mass Spectrometry, *Limnol. Oceanogr.: Methods* **3**, 349–360

Turnbull I.M., Allibone A.H., Forsyth P.J., & Heron D.W., 1994. Geology of the Bull Pass-St Johns Range Area, Southern Victoria Land, Antarctica. Scale 1:50000. Institute of Geological & Nuclear Sciences geological map 14. 1 sheet + 52 p. Institute of Geological & Nuclear Sciences Ltd., Lower Hutt, New Zealand.

Walker G.P.L., 1973. Lengths of Lava Flows. *Phil. Trans. Roy. Soc. of London*, **274,** 107–118.

Warren, G. 1969. Geology of the Terra Nova Bay-McMurdo Sound Area, Victoria Land. Antarctic Map Folio Series 12, Geology, Sheet 14, American Geographical Society, New York.

Williams P.F., Hobbs B.E., Vernon R.H., & Anderson D.E., 1971. The Structural and Metamorphic Geology of Basement Rocks in the McMurdo Sound Area, Antarctica. *J. Geol. Soc. Australia,* **18**, 127–142.

Wilson G., Levy R., Browne G., Dunbar N., Florindo F., Henrys S., Graham I., McIntosh W., McKay R., Naish T., Ohneiser C., Powell R., Ross J., Sagnotti L., Scherer R., Sjunneskog C., Strong C.P., Taviani M., Winter D., & the ANDRILL-MIS Science Team, this volume. Preliminary Integrated Chronostratigraphy of the AND-1B Drill Core, ANDRILL McMurdo Ice Shelf Project, Antarctica. *Terra Antartica.*